

Feat2GS: Probing Visual Foundation Models with Gaussian Splatting

Yue Chen¹ Xingyu Chen¹ Anpei Chen^{1,3} Gerard Pons-Moll^{3,4} Yuliang Xiu^{1,2}

¹Westlake University ²Max Planck Institute for Intelligent Systems

³University of Tübingen, Tübingen AI Center

⁴Max Planck Institute for Informatics, Saarland Informatics Campus

fanegg.github.io/Feat2GS

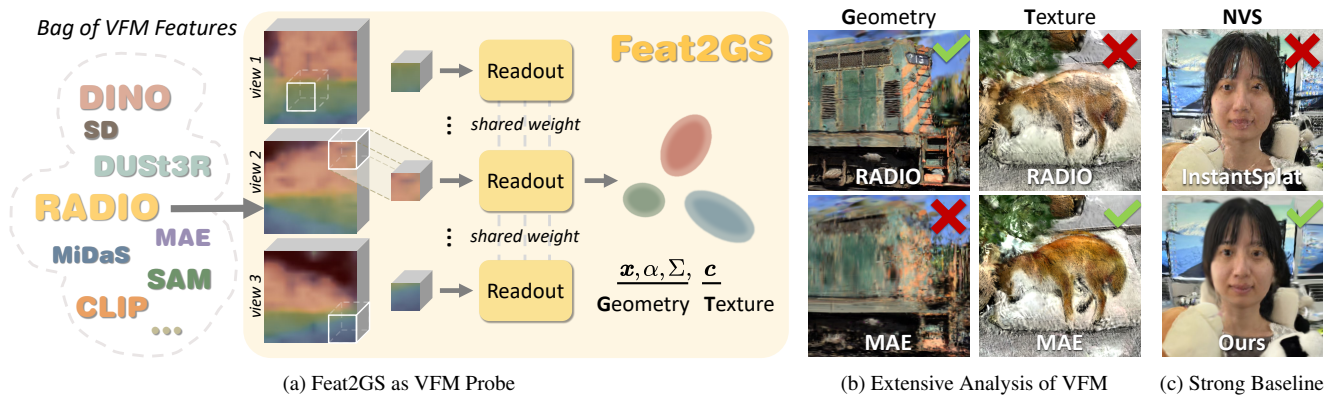


Figure 1. We present **Feat2GS**, a unified framework to probe “texture and geometry awareness” of visual foundation models (VFMs). Novel-view synthesis (NVS) serves as an effective proxy for 3D evaluation. (a) Casually captured photos are input into VFMs to extract features and into a stereo reconstructor to obtain relative poses. Pixel-wise features are transformed into 3D Gaussians (3DGS) using a lightweight readout layer trained with photometric loss. (b) 3DGS parameters, grouped into **Geometry** and **Texture**, enable separate analysis of geometry/texture awareness in VFMs, evaluated by the NVS quality on diverse, unposed open-world images. (c) Our baseline derived from extensive empirical analysis, achieves superior performance for NVS by simply concatenating features from diverse VFMs.

Abstract

Given that visual foundation models (VFMs) are trained on extensive datasets but often limited to 2D images, a natural question arises: how well do they understand the 3D world? With the differences in architecture and training protocols (i.e., objectives, proxy tasks), a unified framework to fairly and comprehensively probe their 3D awareness is urgently needed. Existing works on 3D probing suggest single-view 2.5D estimation (e.g., depth and normal) or two-view sparse 2D correspondence (e.g., matching and tracking). Unfortunately, these tasks ignore texture awareness, and require 3D data as ground-truth, which limits the scale and diversity of their evaluation set. To address these issues, we introduce **Feat2GS**, which readout 3D Gaussians attributes from VFM features extracted from unposed images. This allows us to probe 3D awareness for geometry and texture via novel view synthesis, without requiring 3D data. Additionally, the disentanglement of 3DGS parameters – geometry ($\mathbf{x}, \alpha, \Sigma$) and

texture (\mathbf{c}) – enables separate analysis of texture and geometry awareness. Under **Feat2GS**, we conduct extensive experiments to probe the 3D awareness of several VFMs, and investigate the ingredients that lead to a 3D aware VFM. Building on these findings, we develop several variants that achieve state-of-the-art across diverse datasets. This makes **Feat2GS** useful for probing VFMs, and as a simple-yet-effective baseline for novel-view synthesis. Code and data will be made available at fanegg.github.io/Feat2GS.

1. Introduction

Visual foundation models (VFMs) [6] have emerged as the basis for various 2D reasoning tasks [44, 69] and as a critical component for 3D fine-tuning [3, 10, 13, 34, 39, 70, 94, 106]. Their strong few-shot or zero-shot generalization ability stems mainly from the expressive features [9, 72, 75]. But what is the key for the 3D expressiveness? Does 3D aware-

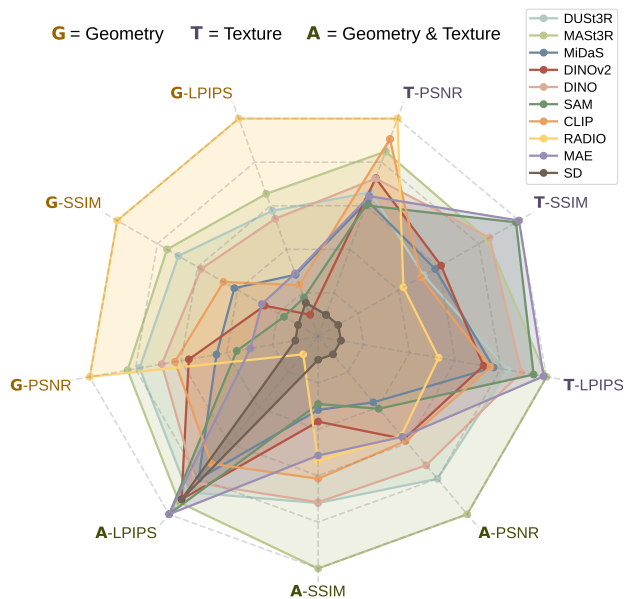


Figure 2. **Texture+Geometry probing of mainstream VFMs.** Normalized average metrics for novel view synthesis (NVS) across six datasets are plotted on axes, with higher values away from the center indicating better performance. Try the interactive visualization demo on fanegg.github.io/Feat2GS.

ness have to come from 3D data? Some VFMs, such as DINOv2 and MAE, are trained using only 2D images. *How important is the training approach?* VFMs differ in many aspects, such as learning strategies (e.g., self-supervised [9, 33], supervised learning [44, 49, 94]), and proxy tasks (e.g., depthmap regression [94], cross-view completion [97], generation [75]). These differences make fair and comprehensive benchmarking difficult.

To answer these questions, recent works [21, 74] evaluate the geometry awareness of VFMs using two proxy tasks: 1) 2.5D depth/normal/token estimation from a single image [21, 74], and 2) 2D matching/tracking between two views [2, 21]. Though it does analyze the 3D awareness of current VFMs, it does not probe the texture awareness and multi-view dense consistency of VFM features, which are critical for 3D-related tasks, such as reconstruction and generation.

For “**texture awareness**”, texture-invariant training improves geometry estimation but can harm texture preservation (see RADIO in Fig. 2). However, recovering original textures from VFM features is key for training on large-scale 2D data with photometric loss [23, 34, 81, 105]. “**Multi-view dense probing**”, like novel view synthesis (NVS) [8, 82], allows every input pixel to contribute to the evaluation, rather than just sparse matching points. Unlike 2D sparse matching, NVS only requires images, eliminating the need for costly labeling of visual correspondences. With the numerous public multi-view datasets [4, 46, 52, 60, 111] available, covering diverse scenes and viewpoints, a new 3D probing approach

Feat2GS	-Geometry	-Texture	-All	InstantSplat [22]
Feature-Readout	x, α, Σ	c	x, c, α, Σ	-
Free-Optimize	c	x, α, Σ	-	x, c, α, Σ

Table 1. **GTA probing schemes.** Unlike InstantSplat, Feat2GS uses shallow readout layer to parse VFM features into 3DGS. GTA modes include: **Geometry**– VFM features to Gaussian geometric parameters (i.e., positions x , opacity α , covariance Σ), **Texture**– VFM features to Gaussian textural parameters, i.e., SH coefficients c , and **All**– all parameters are regressed from features.

using these datasets to evaluate texture and geometry awareness in dense mode could be invaluable.

Thus, we introduce Feat2GS, short for Feature2Gaussian, which evaluates both texture and geometry awareness of VFMs, in the NVS task, using only 2D multi-view data. As shown in Fig. 1, during training, Feat2GS extracts image features from the input views using pre-trained VFMs. A shallow MLP readout layer then regresses the parameters of 3D Gaussians [40] from these features. Multi-view photometric loss minimizes the visual difference between renderings and inputs. During testing, visual similarity metrics (i.e., PSNR, SSIM, LPIPS) are measured for unseen views, across diverse datasets, with Tab. 5 demonstrating that these 2D metrics align well with 3D metrics. To handle sparse and uncalibrated casual images, we initialize camera parameters using DUST3R [94] and refine them with photometric loss.

The parameters of 3DGS, grouped into geometry (x, α, Σ) and texture (c), enable separate analysis of VFM’s texture and geometry awareness. Each group could switch between the “Feature-Readout” and “Free-Optimize” modes to use VFM features as input or free-optimized. This leads to three probing schemes (short as GTA), as shown in Tab. 1.

In summary, our key contributions are as follows:

- 1) Feat2GS as VFM probe.** Feat2GS offers a unified framework (Fig. 1) to probe the 3D awareness (texture and geometry) of pre-trained VFMs, without using 3D labels.
- 2) Extensive analysis of VFM.** We evaluate a wide range of mainstream VFMs (Fig. 2) across diverse multi-view datasets (Tab. 4), spanning from simple scenes to causal captures. These experiments reveal common drawbacks of VFMs and shed light on how to improve them (Sec. 4.3).
- 3) Strong baseline for NVS.** Motivated by these findings, we design three variants of Feat2GS that outperform the current SOTA InstantSplat [22] in all metrics (Tab. 6).

2. Related Work

Measuring 3D Awareness of VFMs. There is no doubt that, visual foundation models [6], short as VFMs, have significantly advanced various 3D vision tasks, such as geometric cue estimation [3, 27, 35, 39, 42, 70, 106], 6D pose estimation [65], visual tracking [88], spatial reasoning [13, 24], and *etc.* However, behind these advances and everyday SOTA records, *are these VFMs truly 3D-aware, even when trained*

without any 3D data? If so, to what extent? And what enables such awareness? There is a line of works that try to answer these questions through multi-view object consistency [7], spatial visual question answering [26, 121], visual perspective taking [53] and robot learning [56, 78, 118]. Although in the same spirit of 3D probing, these existing works mainly focus on coarse-grained semantic reasoning, such as determining “which marker is closer” instead of fine-grained, or even pixel-wise spatial reasoning, like depth estimation. Regarding the fine-grained 3D probes, they either use 2.5D proxy tasks, such as geometric cues estimation (*i.e.*, depth, normal) [21] and view token estimation [74], or use two-view sparse point matching [21] and tracking [2] to assess the 3D awareness of VFMs. The main constraint of these fine-grained 3D probes is their reliance on labeled 3D data, which significantly limits fair and comprehensive evaluation on large-scale visual data. Feat2GS addresses this by first regressing 3DGS from VFM features and then benchmarking 3D awareness via novel view synthesis. This comes with two advantages: ALL raw pixels can contribute to the final evaluation, and ANY multi-view captures can be leveraged. Feat2GS enables “dense” and “diverse” 3D probing.

NVS from Casual Images. Novel view synthesis has made significant progress in recent years [11, 40, 61, 62, 85]. When it comes to sparse and causal captures, which is a quite challenging scenario, various regularizers [63, 102] or visual priors, such as depth [20, 119], pre-trained visual features [36, 101], diffusion priors [96, 98] and feed-forward modeling [10, 12, 17, 34, 38, 54, 76, 89, 110, 120], have been introduced. However, these methods assume known camera poses from Structure-from-Motion [77], which are not available for sparse captures with minimal overlap. Although some works attempt to optimize camera poses alongside NVS optimization [95], using techniques like coarse-to-fine encoding [51], local-to-global registration [16], geometric constraints [37], adversarial objectives [58], dense correspondence [86], and external priors [5, 28, 59], they can only handle dense-view or video-like sequences — not sparse-view images. Groundbreaking methods like DUST3R [94], MAST3R [49], and subsequent works [91, 114] address these limitations by training models on large-scale datasets. They approach the pairwise reconstruction problem as a regression of point maps, easing the strict constraints of traditional projective camera models. This enables “Unconstrained Stereo 3D Reconstruction” of arbitrary image collections, without needing prior information about camera calibration or viewpoint poses. The predicted pointmap can directly initialize 3DGS [40], which can then be regressed in a two-view feedforward [23, 81, 105] or optimized with multi-view photometric losses [22]. InstantSplat [22] closely mirrors our target of optimizing 3DGS from sparse captures using DUST3R estimated cameras. What sets our Feat2GS apart is that we readout 3DGS using visual features, instead of

optimizing it in free form, see Tab. 1. This can be done with a shallow readout MLP, helping to prevent overfitting.

3D Feature Fields. Beyond modeling the appearance, 3D neural fields [99] (*e.g.*, NeRF [61], 3DGS [40]) can also model features, by aggregating 2D features extracted from multiple views into a 3D canonical frame. The feature extractors can either be learned from data [80, 116] in an end-to-end manner, or be off-the-shelf Visual Foundation Models (VFMs), such as DINO [9], CLIP [69], Stable Diffusion [75], SAM [44, 73], and LSeg [50]. Different VFMs equip the 3D feature field with various capabilities: CLIP, and LSeg, which connect language with images, are used by several works [41, 47, 67, 90, 117] to enable text-based querying and editing. SAM, which truly learns the concept of “object”, has been used for grouping [43, 108], segmentation [68, 117], and 3D scene understanding [108, 117]. Meanwhile, the 3D feature fields distilled from DINO and SD show promising cross-instance and cross-frame consistency, as leveraged by FeatureNeRF [107] and N3F [87] for various downstream tasks, such as keypoint transfer, co-segmentation, and video-based object retrieval. Additionally, DINO is also used by LERF [41] and DFFs [47] to regularize CLIP features for finer decomposition.

What sets Feat2GS apart from these 3D feature field works, is their assumption of 3D-awareness and cross-view feature correspondence of VFMs, while Feat2GS questions this: Are they truly 3D-aware? If so, to what extent? Does the 3D-awareness come from color or shape? How can it be improved? Feat2GS provides a unified and neat analysis framework to address these questions, using VFM features for novel-view synthesis, instead of optimizing an additional 3D feature field to align with the 3D radiance field.

3. Method

3.1. Feat2GS

We illustrate our pipeline in Fig. 1. After extracting frozen feature maps from various visual foundation models (VFMs), we take the following steps to ensure fair probing: unifying the feature channel dimensions using Principal Component Analysis (PCA) [32], standardizing the spatial dimensions via bilinear upsampling, and maintaining a consistent network architecture for different VFM features. Specifically, Feat2GS takes the compact features \mathbf{f}_i of each pixel $i \in \{1, 2, \dots, n\}$ as input and output per-pixel Gaussian primitive via a readout layer g_Θ :

$$\mathbf{G}_i = g_\Theta(\mathbf{f}_i), \quad (1)$$

where each Gaussian \mathbf{G}_i is parameterized by: position $\mathbf{x} \in \mathbb{R}^3$, opacity $\alpha \in \mathbb{R}$, covariance matrix $\Sigma \in \mathbb{R}^{3 \times 3}$, and three order of spherical harmonic (SH) coefficients $\{\mathbf{c}_i \in \mathbb{R}^{48} | i = 1, 2, \dots, n\}$.

VFM	Arch.	Channel	Supervision	Dataset
DUST3R [94]	ViT-L/16	1024	Point Regression	3D DUST3R-Mix
MASt3R [49]	ViT-L/16	1024	Point Regression	3D MASt3R-Mix
MiDaS [70]	ViT-L/16	1024	Depth Regression	3D MiDaS-Mix
DINOv2 [64]	ViT-B/14	768	Self Distillation	2D LVD-142M
DINO [9]	ViT-B/16	768	Self Distillation	2D ImageNet-1k
SAM [44]	ViT-B/16	768	Segmentation	2D SA-1B
CLIP [69]	ViT-B/16	512	Contrastive VLM	2D WIT-400M
RADIO [72]	ViT-H/16	1280	Multi-teacher Distillation	2D DataComp-1B
MAE [33]	ViT-B/16	768	Image Reconstruction	2D ImageNet-1k
SD [75]	UNet	1280	Denoising VLM	2D LAION

Table 2. **VFMs for Evaluation.** For fair comparison, we use checkpoints with comparable architectures and training scales, unify the feature channel dimensions via PCA, and maintain a consistent probing network architecture for all VFMs.

To prevent 3D Gaussians from being represented by the readout layer, we constrain the readout layer with a small number of parameters that forcing the 3D Gaussians are decoded from the features. Specifically, the readout layer is constructed using a 2-layer MLP with 256 units per-layer and ReLU activation. Then we splat 3D Gaussians onto images via differentiable rasterization. Note that, to enable our method to evaluate casually captured, sparse, and uncalibrated images, we use an unconstrained stereo reconstructor [49, 91, 114], DUST3R [94] in our experiments, to initialize the camera poses \mathbf{T} , which are then jointly updated with the readout layer Θ using a simple photometric loss between renderings \mathcal{R} and images \mathcal{I} :

$$\min_{\Theta, \mathbf{T}} \|\mathcal{R}(g_{\Theta}(\mathbf{f}), \mathbf{T}) - \mathcal{I}\|. \quad (2)$$

To decouple the geometry and texture awareness, we propose three probing modes: **Geometry** reads out geometric parameters from the 2D image features, and freely optimizes textural parameters \mathbf{c}_i :

$$\{\mathbf{x}_i, \alpha_i, \Sigma_i\} = g_{\Theta}^{(G)}(\mathbf{f}_i) \quad (3)$$

Texture reads out textural parameters, and directly optimizes geometric parameters $\{\mathbf{x}_i, \alpha_i, \Sigma_i\}$:

$$\{\mathbf{c}_i\} = g_{\Theta}^{(T)}(\mathbf{f}_i) \quad (4)$$

All reads out all Gaussian parameters:

$$\{\mathbf{x}_i, \alpha_i, \Sigma_i, \mathbf{c}_i\} = g_{\Theta}^{(A)}(\mathbf{f}_i) \quad (5)$$

3.2. Warm Start

We find that directly decoding 3D structures from 2D image features can easily stuck in local minimal due to the sparse nature of casual images. To ensure robust evaluation of features from diverse foundation models, we warm up our optimization using a point cloud regression:

$$\min_{\Theta} \|g_{\Theta}(\mathbf{f}) - \mathbf{G}_{init}\|, \quad (6)$$

Dataset	Scene Type	Complexity	View Range	Views
LLFF [60]	Indoor	Simple	Small	2
DTU [1]	Indoor Object	Simple	Small	3
DL3DV [52]	Indoor / Outdoor	Moderate	Medium	5-6
Casual	Daily Scenario	Moderate	Medium	4-7
MipNeRF360 [4]	Unbounded	Moderate	360	6
MVingNet [111]	Outdoor Object	Moderate	180-360	2-4
T&T [46]	Indoor / Outdoor	High	Large	6

Table 3. **Datasets for Evaluation.** Classified by scene type, complexity, viewpoint variation, and sampled views.

where \mathbf{G}_{init} refers to the initialization point cloud comes from unconstrained stereo reconstructor.

3.3. Evaluation

We choose to evaluate on NVS from casual (sparse and uncalibrated) images [22] for two main reasons: (1) Diversity. The capability of handling casual images helps diversify the evaluation data by lowering the requirements for acquisition techniques and view setups. (2) Discrepancy. This task poses more of a challenge compared to dense-view NVS, making it better to differentiate the performance of various VFM features. To enable our evaluation to cover arbitrary casual capturing from 3 to N views, we uniformly estimate the camera parameters of both training and test views across all datasets via unconstrained stereo reconstructor. Subsequently, we perform test-time pose optimization [22, 51] via photometric loss to further refine the test poses before evaluating view synthesis quality.

4. Experiments

4.1. Experimental Setup

Features. We focus our experiments on 10 VFMs that show strong potential for generalizable 3D awareness, comparing models trained on different data types (2D vs. 3D) and supervision strategies (*e.g.*, supervised vs. self-supervised, point vs. depth). An overview is provided in Tab. 2, with more details in *Appx.* To make the comparison as fair as possible, we use publicly available checkpoints and select those with comparable architectures and training scales. We also incorporate IUVRGB, comprising image index (I), pixel coordinates (UV), and colors (RGB), as a baseline.

Datasets. To reliably evaluate different features, our experiments utilize seven multi-view datasets, with sparse views sampled spanning from 2 to 7, and test viewpoints far from the training viewpoints. These datasets, as shown in Tab. 3, rich in diversity, provide us with a more comprehensive perspective compared to datasets with 3D ground-truth.

Metrics. We evaluate novel view synthesis across seven datasets using standard metrics: PSNR, SSIM, and LPIPS. For metric calculation, we follow Splatt3R [81] by applying masks to both the rendered and test images. These masks

Feature	LLFF									DL3DV									Casual								
	Geometry			Texture			All			Geometry			Texture			All			Geometry			Texture			All		
	PSNR \uparrow	SSIM \uparrow	LPIPS \downarrow	PSNR \uparrow	SSIM \uparrow	LPIPS \downarrow	PSNR \uparrow	SSIM \uparrow	LPIPS \downarrow	PSNR \uparrow	SSIM \uparrow	LPIPS \downarrow	PSNR \uparrow	SSIM \uparrow	LPIPS \downarrow	PSNR \uparrow	SSIM \uparrow	LPIPS \downarrow	PSNR \uparrow	SSIM \uparrow	LPIPS \downarrow	PSNR \uparrow	SSIM \uparrow	LPIPS \downarrow	PSNR \uparrow	SSIM \uparrow	LPIPS \downarrow
DUST3R	19.88	.7442	.2123	19.01	.7120	.2262	19.87	.7190	.2691	19.64	.7338	.3196	18.01	.6815	.3219	19.39	.7360	.3458	19.29	.6562	.3580	17.54	.5693	.3750	19.19	.6556	.4050
MASt3R	19.89	.7447	.2123	19.01	.7115	.2261	19.99	.7250	.2657	19.64	.7334	.3188	18.07	.6813	.3211	19.41	.7373	.3464	19.30	.6550	.3576	17.59	.5708	.3722	19.37	.6588	.4027
MiDaS	19.81	.7420	.2154	19.00	.7129	.2261	19.86	.7142	.2733	19.47	.7271	.3311	17.94	.6796	.3224	19.22	.7291	.3493	19.24	.6545	.3612	17.52	.5693	.3757	18.96	.6516	.4073
DINov2	19.77	.7345	.2226	19.04	.7133	.2254	19.91	.7163	.2637	19.47	.7293	.3288	18.00	.6805	.3223	19.27	.7317	.3479	19.42	.6524	.3698	17.64	.5701	.3754	19.21	.6535	.4023
DINO	19.81	.7423	.2140	18.98	.7121	.2260	19.97	.7212	.2744	19.60	.7324	.3209	17.97	.6790	.3219	19.41	.7359	.3476	19.24	.6513	.3614	17.50	.5683	.3756	19.10	.6566	.4056
SAM	19.72	.7354	.2181	18.98	.7133	.2260	19.76	.7144	.2629	19.48	.7297	.3271	17.97	.6822	.3218	19.20	.7272	.3459	19.32	.6469	.3704	17.52	.5725	.3736	19.19	.6569	.3981
CLIP	19.78	.7378	.2221	19.02	.7113	.2276	19.74	.7136	.2822	19.53	.7295	.3304	18.05	.6771	.3235	19.22	.7310	.3563	19.21	.6552	.3719	17.46	.5669	.3743	19.05	.6582	.4084
RADIO	19.73	.7402	.2207	19.06	.7101	.2301	19.56	.6999	.3252	19.48	.7313	.3139	18.03	.6748	.3254	19.20	.7316	.3654	19.54	.6545	.3465	17.52	.5666	.3748	18.67	.6533	.4216
MAE	19.75	.7363	.2183	19.00	.7128	.2249	19.92	.7209	.2612	19.54	.7288	.3248	17.98	.6821	.3207	19.34	.7310	.3448	19.03	.6502	.3690	17.51	.5691	.3758	19.18	.6547	.3974
SD	19.62	.7293	.2234	18.85	.7100	.2297	19.78	.7121	.2656	19.31	.7251	.3276	17.79	.6784	.3260	19.10	.7282	.3500	19.24	.6483	.3649	17.38	.5698	.3789	18.86	.6505	.4053
IUVRGB	15.55	.5765	.3986	19.75	.7303	.2292	15.38	.6175	.4308	14.78	.6326	.4541	18.75	.7023	.3250	14.05	.6431	.4386	13.17	.5454	.5248	17.88	.5927	.3846	13.71	.5917	.4955
	MipNeRF 360									MVImgNet									Tanks and Temples (T&T)								
	Geometry			Texture			All			Geometry			Texture			All			Geometry			Texture			All		
Feature	PSNR \uparrow	SSIM \uparrow	LPIPS \downarrow	PSNR \uparrow	SSIM \uparrow	LPIPS \downarrow	PSNR \uparrow	SSIM \uparrow	LPIPS \downarrow	PSNR \uparrow	SSIM \uparrow	LPIPS \downarrow	PSNR \uparrow	SSIM \uparrow	LPIPS \downarrow	PSNR \uparrow	SSIM \uparrow	LPIPS \downarrow	PSNR \uparrow	SSIM \uparrow	LPIPS \downarrow	PSNR \uparrow	SSIM \uparrow	LPIPS \downarrow	PSNR \uparrow	SSIM \uparrow	LPIPS \downarrow
DUST3R	20.82	.5008	.3795	19.10	.4489	.3816	21.02	.5048	.4752	19.47	.6004	.3073	16.88	.5348	.3334	19.43	.5937	.3674	18.85	.6458	.3715	17.53	.6222	.3328	18.61	.6477	.4023
MASt3R	20.92	.5093	.3745	19.21	.4540	.3803	20.92	.5054	.4749	19.49	.6008	.3032	16.91	.5350	.3337	19.49	.5983	.3637	18.80	.6428	.3703	17.68	.6238	.3319	18.76	.6512	.3991
MiDaS	20.89	.5059	.3815	19.05	.4509	.3813	20.84	.5004	.4795	19.35	.5900	.3222	16.82	.5336	.3343	19.34	.5910	.3672	18.53	.6374	.3798	17.64	.6238	.3333	18.32	.6428	.4039
DINov2	20.81	.4946	.3953	19.05	.4495	.3821	20.75	.4924	.4684	19.35	.5896	.3246	16.88	.5359	.3344	19.43	.5943	.3674	18.71	.6432	.3772	17.58	.6214	.3348	18.43	.6443	.4064
DINO	20.91	.5054	.3769	19.18	.4545	.3795	20.83	.5010	.4772	19.44	.5982	.3071	16.90	.5394	.3329	19.41	.5952	.3683	18.75	.6416	.3733	17.66	.6233	.3330	18.61	.6467	.4030
SAM	20.73	.4913	.3945	19.14	.4556	.3775	20.75	.4949	.4639	19.23	.5899	.3188	16.84	.5346	.3346	19.29	.5915	.3649	18.65	.6421	.3780	17.49	.6217	.3338	18.43	.6425	.4029
CLIP	20.80	.4982	.3913	19.28	.4543	.3807	20.88	.4984	.4773	19.41	.5945	.3098	16.96	.5362	.3358	19.37	.5969	.3695	18.92	.6463	.3729	17.81	.6226	.3316	18.75	.6515	.4052
RADIO	20.87	.5100	.3620	19.35	.4550	.3819	20.91	.5067	.5127	19.54	.6105	.2949	16.99	.5373	.3366	19.60	.5955	.3946	19.19	.6612	.3480	17.84	.6225	.3321	19.01	.6574	.4109
MAE	20.82	.4992	.3884	19.14	.4572	.3781	20.79	.4995	.4668	19.23	.5909	.3142	16.84	.5355	.3328	19.25	.5914	.3680	18.65	.6395	.3758	17.55	.6234	.3333	18.49	.6451	.4000
SD	20.71	.4962	.3985	18.89	.4472	.3839	20.59	.4929	.4672	19.08	.5881	.3185	16.63	.5313	.3389	19.06	.5838	.3660	18.69	.6422	.3772	17.32	.6217	.3374	18.55	.6467	.4020
IUVRGB	16.45	.4075	.5910	19.96	.4797	.3911	16.41	.4187	.5929	14.83	.5069	.4648	17.84	.5568	.3431	15.38	.5362	.4699	15.29	.5846	.4736	18.60	.6526	.3396	15.17	.5948	.4718

Table 4. **Quantitative Results.** We evaluate geometry and texture awareness of VFMs on NVS using Geometry, Texture, and All probing modes. Results indicate that VFM performance varies across datasets, highlighting the importance of dataset diversity. The lack of texture awareness in VFMs limits both Texture mode and All mode, especially in LPIPS. Performance is ranked by color, from worst to best.



Figure 3. **Qualitative Examples.** We compare novel view renderings across VFM features. In Geometry mode, the multi-teacher-distillation method (RADIO) and point-regression-based methods (MASt3R, DUST3R) produce more plausible geometry, *e.g.*, vehicle front and the wheel, indicating better multi-view consistency. All VFM features struggle in Texture mode, and renderings in the All mode are notably blurred, both reflecting the limited texture awareness of current VFMs.

define valid pixels as those inside the frustum of at least one view and with reprojected depths aligned with DUST3R predicted depth. All metrics are computed over the entire image. On the DTU dataset, we measure the distance between reconstructed 3DGS and point cloud ground truth (Tab. 5), reporting average accuracy, completeness, and distance, as in prior works [1, 91]. Accuracy is the smallest Euclidean distance from a reconstructed point to ground truth, and completeness is the smallest Euclidean distance from a ground-truth point to the reconstruction. Distance is the Euclidean distance based on ground-truth point matching.

Implementation Details. Feat2GS is implemented with PyTorch [66] and gsplat [109]. For fair probing, images are resized to 512, reduced to 256 channels with PCA, then

upsampled back to 512. We use a 2-layer ReLU MLP for g_{Θ} with 256-dimensional hidden units. Adam optimizer is used to optimize the parameters of MLP, 3D Gaussians, and cameras. At the warm start stage, we optimize the MLP parameters for 1K iterations with a learning rate that starts at 1×10^{-2} and decays exponentially to 1×10^{-4} . After this stage, optimization continues for another 7K iterations. We follow the learning rate strategy of vanilla 3DGS [40]. For the MLP part, we maintain the original ratio but reduce the learning rate by an order of magnitude. To optimize the cameras, the learning rate starts at 1×10^{-4} and decays exponentially to 1×10^{-6} at 1K iteration. All experiments are conducted on a single NVIDIA GeForce RTX 4090 GPU.

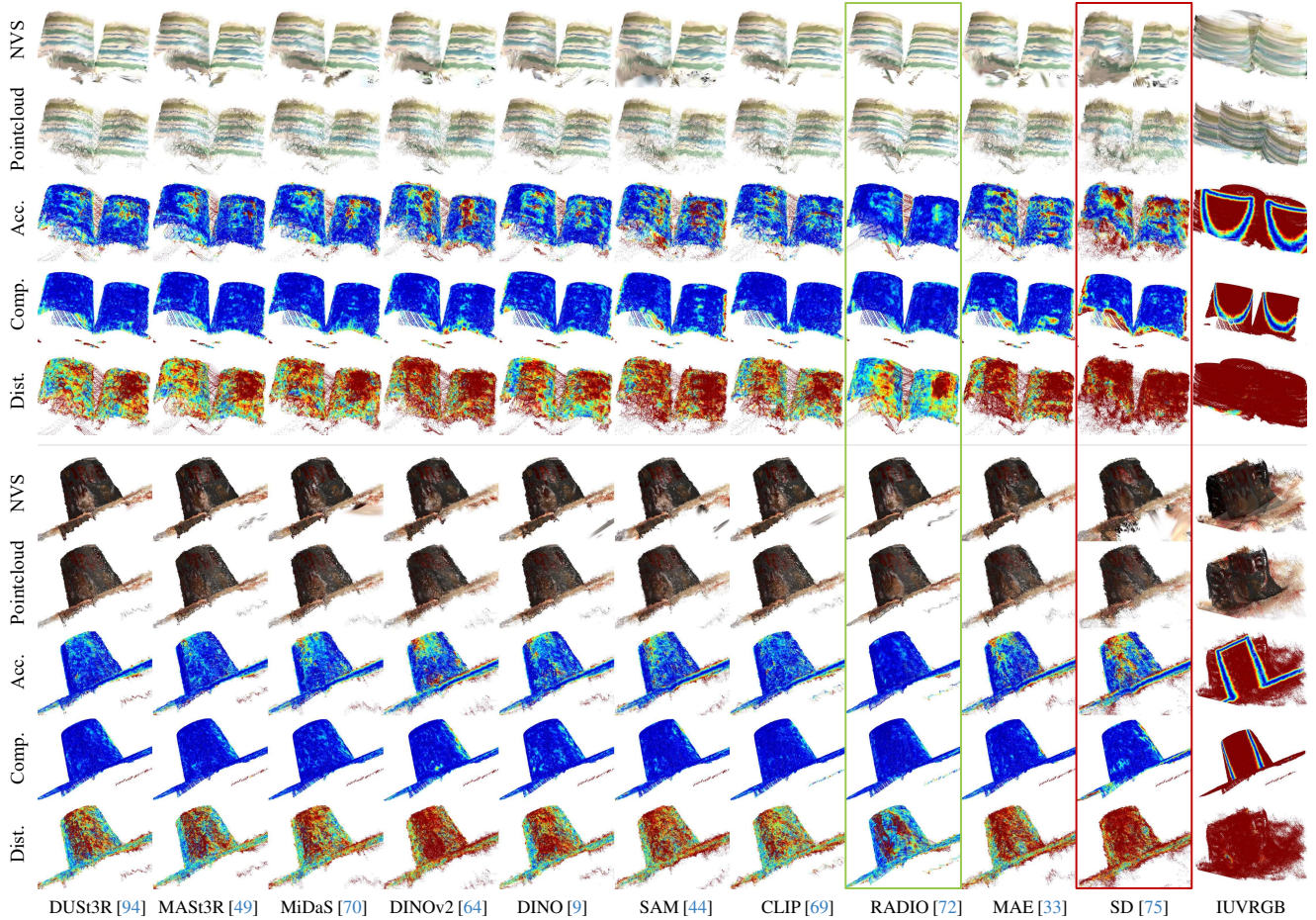


Figure 4. **Novel View Synthesis as Proxy Task to Assess 3D.** We present qualitative examples from the DTU dataset, including NVS, Pointcloud (readout 3DGS positions), Accuracy (smallest distance from a readout point to ground-truth), Completeness (smallest distance from a ground-truth point to a readout point), and Distance (based on ground-truth point matching). Results show that NVS quality aligns with 3D metrics, proving its reliability as an indicator for 3D assessment. RADIO performs best, SD worst, with IUVRGB as a reference. **Q Zoom in** or check our [video](#) to see more details.

Feature	2D Metrics			3D Metrics		
	PSNR \uparrow	SSIM \uparrow	LPIPS \downarrow	Acc. \downarrow	Comp. \downarrow	Dist. \downarrow
DUS3R	21.36	.7772	.2195	2.439	1.316	6.955
MAS3R	21.44	.7792	.2177	2.321	1.286	6.557
MiDaS	21.09	.7712	.2254	2.934	1.412	8.230
DINOv2	21.01	.7695	.2277	3.101	1.337	8.588
DINO	21.40	.7783	.2187	2.440	1.316	6.885
SAM	20.93	.7660	.2304	3.176	1.339	8.785
CLIP	21.26	.7752	.2215	2.357	1.209	6.739
RADIO	21.78	.7871	.2042	1.886	1.326	5.431
MAE	20.96	.7666	.2289	2.963	1.337	8.374
SD	20.76	.7638	.2343	4.334	1.603	11.594
IUVRGB	16.09	.6825	.3134	13.015	16.957	46.671

(a) 2D Metrics vs. 3D Metrics

3D Metrics	2D Metrics			3D Metrics		
	PSNR	SSIM	LPIPS	Acc.	Comp.	Dist.
Dist.	1.00	1.00	1.00	0.95	0.80	0.96
Comp.	1.00	1.00	1.00	0.95	0.80	0.96
Acc.	1.00	1.00	1.00	0.95	0.80	0.96
PSNR	0.95	0.95	0.95	1.00	0.83	0.99
SSIM	0.80	0.80	0.80	0.83	1.00	0.84
LPIPS	0.96	0.96	0.96	0.99	0.84	1.00

(b) Correlation Matrix

Table 5. **Novel View Synthesis Aligns Well with 3D Metrics.**

(a) We report NVS quality and the Euclidean distance between reconstructed 3DGS positions and pointcloud ground truth on the DTU dataset. (b) Strong 2D-3D metric correlation supports NVS as a benchmark for 3D assessment.

4.2. Motivation Validation

Novel View Synthesis Correlates with 3D Metrics. Using 2D metrics instead of 3D ones allows us to bypass the need for 3D ground-truth. Motivated by this, we propose Feat2GS to assess the 3D awareness of VFMs through the 2D metric of novel view synthesis (NVS). The key question is: *Can novel view synthesis effectively serve as a proxy for 3D metrics?* We posit that high-quality NVS strongly correlates with an accurate 3D representation. To validate this hypothesis, we conduct experiments on the DTU dataset [1] with dense pointclouds as 3D ground-truth, evaluating both the 2D NVS and the 3D point cloud regression tasks. We then calculated the correlation between these results, as shown in Tab. 5. The results reveal a strong correlation between 2D and 3D metrics, supporting NVS as an indicator for 3D assessment. We further qualitatively demonstrate this cor-

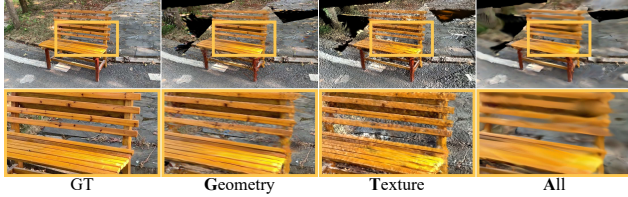


Figure 5. **GTA Modes Comparison for the Same Region.** We present novel view synthesis of GTA modes using RADIO features. **Texture** mode shows broken structures as it excludes VFM features for 3DGS geometry regression, while **All** mode is blurrier than **Geometry** mode due to reliance on VFM features for color regression. This highlights that the blurriness in the **All** mode arises from the lack of texture awareness in VFMs.

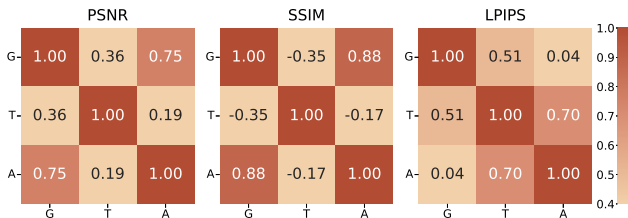


Figure 6. **Performance Correlations of GTA across All Datasets.** The **All** mode correlates strongly with **Geometry** mode in PSNR and SSIM (primarily reflect structural consistency), and is closely related to **Texture** mode in LPIPS (commonly used to assess image sharpness), suggesting an optimal **All** mode depends on both high-performing **Geometry** and **Texture** mode.

relation in Fig. 4. The results indicate a strong relationship between NVS and 3D metrics, confirming that high-quality NVS aligns closely with accurate 3D representations.

Data Diversity Matters for Comprehensive Probing. Testing on small-scale data can lead to biased conclusions. As shown in Tab. 4, the evaluation results vary across probing GTA modes and different datasets. For instance, LLFF is relatively simple for novel view synthesis due to its dense view capturing and small scale. MAST3R, DUST3R, and DINO show superior geometry results on LLFF. However, none of them ranks higher than RADIO on T&T dataset, which features more challenging scenes. Dataset evaluation bias is inevitable. By removing the need for 3D ground truth, we can evaluate on large-scale diverse captures, thereby ensuring that the results are much less biased.

4.3. Findings

Overall Performance. Table 4 benchmarks VFM features with three probing modes: **Geometry**, **Texture** and **All**. The mean scores across diverse datasets are plotted in Fig. 2. The top three performers in **Geometry** mode are RADIO > MAST3R > DUST3R. However, they show significantly different rating in **Texture** mode, with MAE > SAM > MAST3R. In the **All** mode, MAST3R and DUST3R achieve



Figure 7. **Texture Blurriness Comparison.** MAE preserves sharper texture over RADIO. IUVRGB is shown for reference.



Figure 8. **MAE vs. SD on Texture Awareness.** While both MAE and SD are trained to reconstruct images (MAE in pixel space with an MSE loss and SD in feature space with a denoising loss), SD tends to result in a significant color shift.

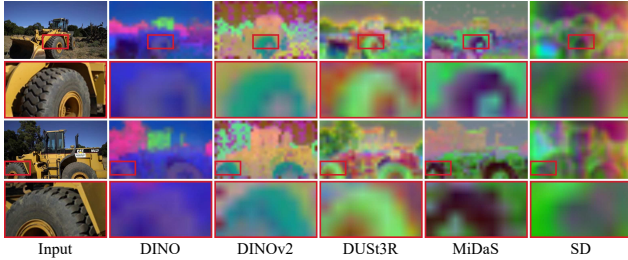
the best score, followed by DINO. In Tab. 4, Stable Diffusion (SD) performs the worst in most metrics, Fig. 3-A shows its significant color drift and broken geometry, check *Appx.* for more qualitative results of geometry. This aligns with the conclusion about SD in Probe3D [21]. Large view-point changes cause inconsistency in the feature space (see Fig. 9b). In the following sections, we provide a comprehensive analysis of the insights behind the above ratings.

Texture-unfriendly Training Strategies. As shown in Tab. 4 and Fig. 3, VFM features perform poorly in **Texture** mode, even worse than the simple IUVRGB encoding shown in Fig. 7. It suggests that current VFM features lack texture awareness, as noted in [81, 105]. One likely explanation for this is that VFMs are often trained for semantic understanding or 3D estimation, which require texture-invariant features to avoid shortcuts [29, 30]. For example, DUST3R is trained to be texture-invariant for better 3D robustness on diverse in-the-wild captures. Heavy data augmentations in SSL (*i.e.*, DINO [9], BYOL [31], SimCLR [14]), such as color jittering, Gaussian blur, and solarization, encourage the model to produce consistent outputs despite changes in appearance or lightning. Since CLIP is trained on weakly aligned image-text pairs, it often includes ambiguous and coarse semantics that are not discriminative enough to model low-level visual patterns, like colors, materials, and textures [92]. RADIO distills DINO and CLIP, achieving excellent geometry awareness, but also inherits their poor texture awareness (see Fig. 2 and Fig. 7).

Texture Benefits from Masked Image Reconstruction. Table 4 shows that the **All** mode is impeded by **Texture** mode, leading to worse performance in LPIPS (by an average of +0.05) than **Geometry** mode, which does not use VFM fea-



(a) NVS Comparison on Geometry Awareness



(b) VFM Features from Training Views

Figure 9. **Feature Consistency Reflected in NVS.** (a) RADIO, MAST3R, DUST3R, and DINO effectively capture geometry. (b) DINO is consistent across training views, but PE artifacts appear in DINOv2. 3D data proves beneficial, as DUST3R is consistent; however, MiDaS shows inconsistency, suggesting that pointmap representation is more reasonable than depth. SD also exhibits inconsistency. These inconsistencies lead to poor NVS.

tures for 3DGS color regression. Terrible texture awareness prevents RADIO from being versatile, as Fig. 2 shows. Visually, as displayed in Fig. 3, novel view renderings in the All mode tends to appear blurred. Figure 5 also shows that Texture mode, which excludes VFM features for 3DGS geometry regression, exhibits broken structures, while All mode appears more blurred than the same regions in Geometry mode because All mode relies on VFM features for 3DGS color regression, unlike Geometry mode, which freely optimizes colors. To further analyze the mutual correlation of GTA modes, we compute their correlation matrix using average metrics across all datasets, as shown in Fig. 6. Results indicate that the All mode is more strongly correlated with Geometry mode in PSNR and SSIM, which primarily reflect structural consistency, but is more closely related to Texture mode in LPIPS, a metric used to evaluate image sharpness. This further supports the notion that the blurriness observed in the All mode stems from a lack of texture awareness in VFMs. Texture is obviously crucial for photorealism. How can it be retained in VFMs? As illustrated in Fig. 2, VFMs with masked-image-reconstruction pre-training (*i.e.*, MAE, MAST3R, DUST3R) rank top in T-LPIPS, and Fig. 7 backs this. MAE’s ability to recover

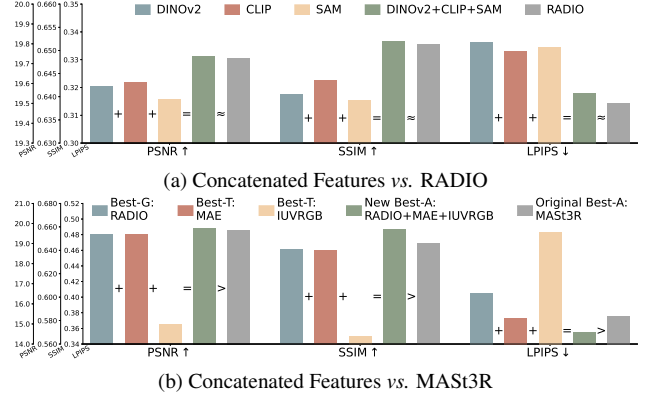


Figure 10. **Feature Concatenation.** (a) RADIO, distilling DINOv2, CLIP, and SAM, achieves superior geometry awareness. Geometry mode with concatenated features from the three yields results comparable to RADIO. (b) The All mode using concatenated VFM features from best Geometry mode and Texture mode, outperforms the original best All mode. +: Feature concatenation; ≈: Comparable performance; >: Superior performance.

sharp textures might be attributed to using only *cropping-only* augmentation. Color jittering degrades results, so it’s not included [33]. Additionally, denoise-based image reconstruction leads to color shift, as shown in Fig. 8.

Geometry Benefits from 3D Data. In Fig. 2, RADIO, MAST3R, DUST3R and DINO rank among the top-4 in geometry awareness metrics. In Fig. 9a, these four features help reconstruct a more complete structure of the excavator, whereas others result in floating artifacts and distortion. Better geometry awareness implies stronger cross-view consistency, which is also supported by Fig. 9b. *What is the key ingredient to achieve geometry awareness? One crucial factor is 3D data.* Both of MAST3R and DUST3R are trained with pointmap. What about 2.5D data, like depth or normal maps? It is much worse, see DUST3R vs. MiDaS at Fig. 9a. Please note that, MiDaS and DUST3R shares the same ViT-L/16 encoder architecture (see Tab. 2) and comparable training scales (3M vs. 2M). The depth map estimation may cause inconsistent features for the same object when viewed from different distances. In contrast, pointmap regression [94] encourages the network to generate consistent features across views, as the scene coordinates remain unchanged when the view changes [8, 79].

Model Ensembling Help. RADIO, distilling DINOv2, CLIP and SAM into a single model, achieves the best geometry awareness, as shown in Figs. 2, 3 and 9a. A natural question arises: *Could simply concatenating these features yield comparable results? Yes!* Specifically, we concatenate features of DINOv2, CLIP and SAM, and then apply PCA to reduce feature channels to 256, keeping the size of the network unchanged for a fair comparison. Fig.



Figure 11. **NVS from Casual (Sparse and Uncalibrated) Images.** We compare our Geometry mode baselines against InstantSplat, which overfits to training views and results in broken structures. Feat2GS with RADIO produces more consistent results due to alignment from features and compact readout. Concatenating all VFM features leads to more complete geometry, *e.g.*, auditorium seat backs (X-shaped gaps vs. straight-line gaps), while fine-tuned DUST3R* features further refine details, *e.g.*, signage.

Method	All Datasets		
	PSNR \uparrow	SSIM \uparrow	LPIPS \downarrow
InstantSplat [22]	18.87	0.6044	0.3039
Feat2GS w/ RADIO	19.73	0.6513	0.3143
Feat2GS w/ concat all	19.80	0.6545	0.3105
Feat2GS w/ DUST3R	19.66	0.6469	0.3247
Feat2GS w/ DUST3R*	19.75	0.6561	0.2928

Table 6. **Baselines of Feat2GS** in NVS from casual (sparse and uncalibrated) images. We compare Geometry mode with RADIO features, concatenation of all VFM features, DUST3R, and fine-tuned DUST3R* features against the current SOTA InstantSplat.

ure 10a shows that, in Geometry mode, feature concatenation (DINOv2+CLIP+SAM) outperforms model distillation (RADIO). This inspires us to further explore: *What if we combine the best Geometry mode feature and the best Texture mode feature?* Figure 6 has indicated that the optimal All mode should have no weakness in either texture or geometry. As shown in Fig. 10b, the All mode using concatenated features from RADIO (best in Geometry mode) with MAE and IUVRGB (best in Texture mode), outperforms the original best All mode with MAST3R features. This exploration shows the potential of our probing method.

5. Application

Feature Pickup. Inspired by Sec. 4.3, we make three Feat2GS variants to compare with InstantSplat [22], in the NVS task using casual (sparse and uncalibrated) images. Specifically, we pick up the TOP1 of Geometry mode, RADIO, as the first baseline. As shown in Tab. 6, Feat2GS with RADIO features achieves better PSNR and SSIM over InstantSplat. The qualitative results in Fig. 11 show that InstantSplat often produces broken structures and discontinuity artifacts. This occurs because optimizing millions of 3DGS for sparse viewpoints leads to overfitting high-

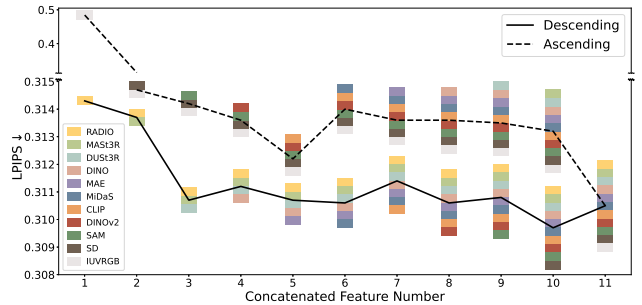


Figure 12. **Ranking-Ordered Feature Concatenation.** Based on performance on Geometry mode, VFM features are ranked and concatenated in two orders: descending (best to worst) and ascending (worst to best). Performance improves with more concatenated features and with higher-ranking features.

frequency details, resulting in suboptimal parameters. In contrast, Geometry mode of Feat2GS with RADIO features can produce higher-quality synthesized novel views, thanks to RADIO’s strong geometry awareness. This allows us to read out 3DGS from the deep features using a very lightweight (2-layer) MLP, which is crucial for avoiding overfitting.

Feature Ensembling. Since simple feature concatenation is effective (see Fig. 10), it makes sense to consider a straightforward approach: concatenating different VFM features. However, exploring all possible feature combinations is impractical. Thus, we rank the features based on Geometry mode performance, and concatenate them in descending (from best- to worst-performing) and ascending (from worst- to best-performing) orders, followed by PCA to reduce the feature dimensions to 256. The results are in Fig. 12. The curve indicates that performance improves as more VFM features are concatenated, with additional gains when higher-ranking VFM features are merged. Based on this observation, we simply concatenate all VFM features as our second baseline. Compared to using only RADIO

features, as shown in Fig. 11, “Feat2GS w/ concat all” yields better results. For example, with RADIO features, the auditorium seat backs show X-shaped gaps, whereas concat-all model correctly recover the straight-line gaps between them. Quantitative Tab. 6 also show improvements compared to Feat2GS based on RADIO features, yet it still falls short of InstantSplat in terms of LPIPS. This limitation mainly arises from the low-resolution features extracted from VFM encoders [25, 84]. Though the feature upsampler [25] is leveraged to improve the spatial resolution of features, it does not bring much benefits (detailed in *Appx.*).

Feature Finetuning. Lastly, we explore whether feature fine-tuning during the warm-start stage is beneficial. The results after fine-tuning different VFM features showed minimal differences, indicating that fine-tuning is effective with any well-initialized features (detailed in *Appx.*). Since we use DUST3R to warm-start the readout layer, for simplicity, we compare vanilla DUST3R with fine-tuned DUST3R* at Tab. 6. Feature fine-tuning could improve NVS. Figure 11 demonstrates a clear improvement over SOTA InstantSplat.

6. Limitations and Future Works

Feat2GS has several limitations. First, Feat2GS requires initialization of camera pose and pointclouds estimated by unconstrained stereo reconstructor [49, 91, 114]. While existing methods, DUST3R [94] in our case, are robust for initialization, failures sometimes occur. Although Feat2GS can handle noisy initialization pointcloud, it struggles with those containing significant outliers, as shown in Fig. 13. An exciting direction is to remove this dependence by leveraging VFM features to initialize poses [65] and pointcloud [8]. Second, Feat2GS is designed for controlled settings where scenes are captured in a short time frame under constant lighting. This limits its ability to handle long-term, in-the-wild datasets, where images might be captured hours or years apart, such as internet photo collections of landmarks [83, 89]. Many works [15, 48, 57, 100, 113] show that gradients from differentiable rendering are helpful in this case. Extending Feat2GS with these unconstrained formulations could lead to lifelong in-the-wild probing. Lastly, due to its reliance on 3D Gaussian Splatting, Feat2GS is currently limited to static scenarios. This is a reasonable assumption for evaluation in multi-view image collections, but restricts assessment in dynamic videos. 4D Gaussian Splatting [55, 93] may be used to overcome this limitation.

7. Conclusion

We now return to our original question: Are visual foundation models (VFMs) aware of geometry and texture? To give an answer based on diverse datasets, we proposed Feat2GS, a method that maps features of VFMs to 3DGS, allowing us to explore their geometry and texture awareness through

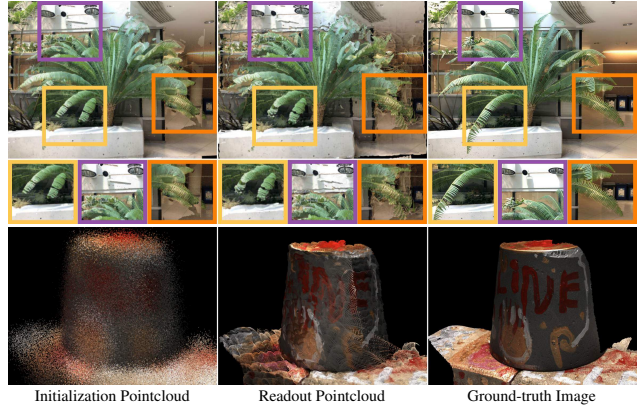


Figure 13. **Failure Case.** Feat2GS can handle noisy initialization pointcloud (bottom row), but it struggles when the initialization pointcloud contains significant outliers (top row), e.g., severely displaced branches (yellow), misplaced lamps (purple), and missing parts of branches (orange). These prevent plausible pointcloud readouts, even with the best geometry-aware VFM feature, RADIO.

2D images without requiring 3D ground-truth. We found that recent VFMs capture geometry well but struggle with texture. 3D pointmap [94] is critical, to learn a multi-view consistent, geometry-aware model. Texture awareness benefits a lot from masked-image-reconstruction pre-training, like MAE [33]. In addition, Feat2GS effectively harnesses VFMs for novel view synthesis (NVS) task on casual, sparse captures. These findings suggest that predicting 3D Gaussians from various views in a canonical space and training the model with photometric loss is a promising strategy for developing 3D VFMs, also noted at [23, 105]. Moreover, VFM feature ensembling is also an interesting topic worth exploring [72, 78], and we demonstrate that this can be effectively achieved in Feat2GS through simple concatenation. We hope these insights, along with Feat2GS—a versatile tool for future model exploration—will advance VFM research and drive progress in 3D vision.

Acknowledgments. We thank *Yuxuan Xue, Vladimir Guzov, Garvita Tiwari* for their valuable feedback, and the members of *Endless AI Lab* and *RVH (Real Virtual Humans)* for their help and discussions. *Yuliang Xiu* has received funding from the European Union’s Horizon 2020 research and innovation programme under the Marie Skłodowska-Curie grant agreement No.860768 (*CLIFE* project). *Yue Chen* and *Xingyu Chen* are supported by the Research Center for Industries of the Future (RCIF) at Westlake University, and the Westlake Education Foundation. *Prof. Gerard Pons-Moll* is a member of the Machine Learning Cluster of Excellence, EXC number 2064/1 - Project number 390727645, and is endowed by the Carl Zeiss Foundation.

Appendices

In the following, we provide implementation details (Sec. A), more quantitative and qualitative results and analysis (Sec. B). Please check the [video](#) for an overview of our framework and more results.

A. Implementation Details

All images are resized to 512 for VFM feature extraction. PCA reduces the feature channels to 256, and then the feature map resolution is upsampled to 512. The DUST3R [94] checkpoint at 512 resolution initializes the point clouds and camera parameters. Photometric loss is computed at the original image resolution. Adaptive density control [40] is omitted throughout the optimization process.

Feat2GS evaluates a total of 11 models, as listed below:

- **Raw Image Feature.** IUVRGB includes image index (I), pixel coordinates (UV), and colors (RGB), serving as a baseline for comparison.
- **Supervised 3D VFMs.** DUST3R [94], MAST3R [49] and MiDaS [70] are trained with pointmap regression, matching, and depth estimation objective using 3D datasets.
- **Self-supervised 2D VFMs.** DINO [9] and DINOv2 [64] are trained with discriminative self-supervised objective using 2D datasets without annotations.
- **Supervised 2D VFMs.** SAM [44] and CLIP [69] are trained with segmentation and contrastive objective using 2D datasets and corresponding annotations.
- **Distilled 2D VFMs.** RADIO [72] merged DINOv2, SAM, and CLIP via model distillation on 2D data.
- **Image-reconstruction-based 2D VFMs.** MAE [33] and Stable Diffusion (SD) [75] are trained with Mean Square Error (MSE) and denoising objective using 2D datasets to reconstruct images in pixel and feature space.

B. Additional Results

Visualization of Depth and Normal. In Sec. 4.3, we identify the top four performers in Geometry mode as RADIO > MAST3R > DUST3R > DINO, while Stable Diffusion (SD) performs the worst, exhibiting broken geometry. We then present qualitative results of geometry with expected depth and normal rendering in Fig. R.1. Additionally, we show the 2.5D renderings of Feat2GS application baselines in Fig. R.2, both illustrating the strong correlation between NVS and depth/normal 2.5D metrics.

Feature Upsampling vs. Fine-tuning. As discussed in Sec. 5, the low-resolution features extracted from VFM encoders limit Feat2GS application baselines in rendering high-frequency details. We then compare two solutions to address this: feature upsampling (using VFM feature upsampler [25] to improve the feature resolution) and feature

Feature	All Datasets								
	Geometry			Texture			All		
	PSNR \uparrow	SSIM \uparrow	LPIPS \downarrow	PSNR \uparrow	SSIM \uparrow	LPIPS \downarrow	PSNR \uparrow	SSIM \uparrow	LPIPS \downarrow
DINOv2	19.59	.6406	.3364	18.03	.5951	.3291	19.50	.6388	.3760
DINOv2 ⁺	19.67	.6480	.3202	18.10	.5950	.3291	19.58	.6443	.3894
DINOv2*	19.78	.6552	.2962	18.18	.5968	.3232	19.80	.6614	.3247
DINO	19.63	.6452	.3256	18.03	.5961	.3282	19.55	.6427	.3793
DINO ⁺	19.72	.6485	.3207	18.03	.5941	.3291	19.64	.6465	.3839
DINO*	19.74	.6557	.2918	18.09	.5949	.3235	19.69	.6630	.3154
CLIP	19.61	.6436	.3331	18.10	.5947	.3289	19.50	.6416	.3832
CLIP ⁺	19.68	.6466	.3222	18.09	.5941	.3286	19.63	.6468	.3842
CLIP*	19.70	.6540	.2959	18.19	.5962	.3242	19.67	.6599	.3199

Table R.1. **Feature Upsampling⁺ vs. Fine-tuning***. We report a quantitative comparison of Feat2GS application baselines between feature upsampling using the recent VFM feature upsampler [25] and feature fine-tuning during the warm-start stage. While feature upsampling offers some benefits, fine-tuning achieves significantly higher improvement, particularly in the LPIPS metric.

fine-tuning (optimizing features during the warm-start stage). As shown in Fig. R.3 and Tab. R.1, upsampling offers little improvement, while feature fine-tuning yields significantly better results. Similar fine-tuning performance across various VFM features shows that fine-tuning increases resolution and enriches embedded information, allowing high-quality reconstruction with any well-initialized features.

Visualization of Two Geometry Awareness Attributes.

We provide qualitative examples in Fig. R.4 to visualize two attributes of geometry awareness. Position \mathbf{x} awareness is highlighted by the sharpness of readout details and edges, while covariance Σ awareness reflects in plane flatness.

Zero123 Outperforms SD in Objaverse-like Scenes.

While Stable Diffusion (SD) performs poorly in most metrics due to its lack of multi-view consistency, does Zero123, which fine-tunes SD on Objaverse [19] multi-view dataset, achieve better cross-view consistency? As shown in Tab. R.2, Zero123 excels in Objaverse-like simple scenes (LLFF) but struggles with complex scenarios (Tanks and Temples), which might be attributed to catastrophic forgetting [45].

DINO captures geometry well but PE artifacts hinder.

In Sec. 4.3, we observe that DINO features capture geometry well, completely reconstructing the vehicle front (Fig. 3) and wheel (Fig. 9a). In contrast, DINOv2 exhibits floating artifacts and distorted structures, likely caused by positional embedding (PE) artifacts noted in recent research [103, 104], as shown in Fig. 9b. We observe that the artifacts in DINOv2’s features lead to degraded performance—an issue that becomes apparent when using a 2-layer MLP but is masked by the DPT head [71] utilized in prior work [21]. This explains why DINO outperforms DINOv2 in Feat2GS, but the opposite occurs in Probe3D [21] and suggests that while DPT can mitigate this issue, it persists and requires solutions such as registration [18], denoising [104], and 3D-aware training [112, 115] to be fundamentally addressed.

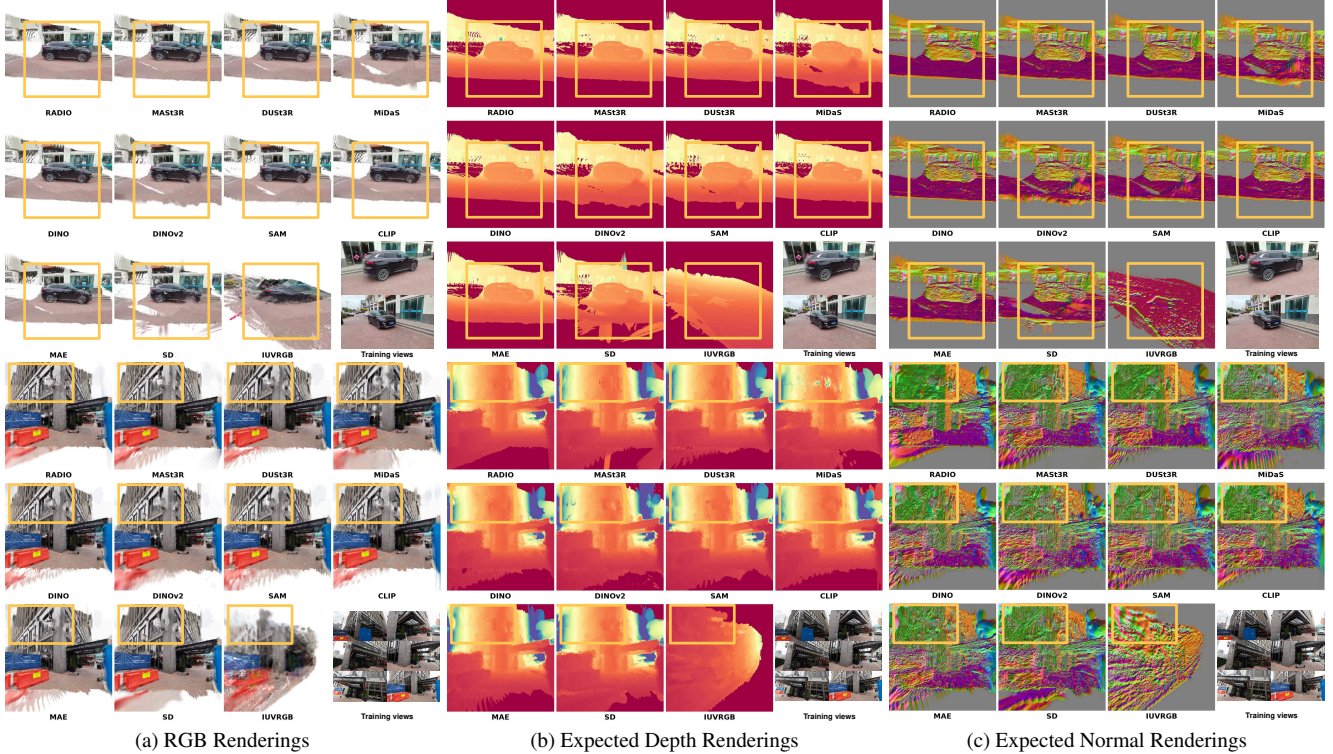


Figure R.1. **Novel View Synthesis of RGB Correlates with Depth and Normal.** We present qualitative examples, including RGB renderings, expected depth renderings, and expected normal renderings, of Geometry mode with different VFMs. This demonstrates that the NVS quality of Feat2GS probing results closely aligns with 2.5D metrics.

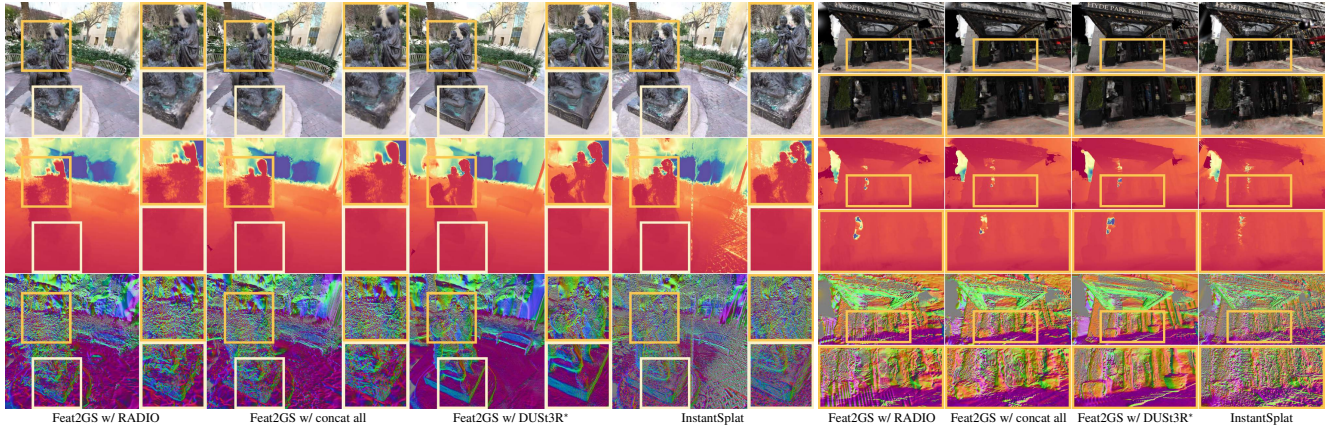


Figure R.2. **Novel View Synthesis of RGB Correlates with Depth and Normal.** We show qualitative examples, including RGB renderings, expected depth renderings, and expected normal renderings, of Geometry mode with different Feat2GS application baselines: feature pickup (Feat2GS w/ RADIO), feature ensembling (Feat2GS w/ concat all), and feature fine-tuning (Feat2GS w/ DUST3R*). This demonstrates that the NVS quality of Feat2GS application baselines closely aligns with 2.5D metrics.

Texture Benefits from Image-Matching-Based Training. Both DUST3R and MAST3R utilize CroCo [97], pre-trained through cross-view completion similar to MAE [33], enabling DUST3R and MAST3R to exhibit texture awareness. But why does MAST3R outperform DUST3R on

Texture mode (see Fig. 3)? One possible explanation is that MAST3R incorporates an additional image matching loss, promoting better awareness of fine-grained textures.

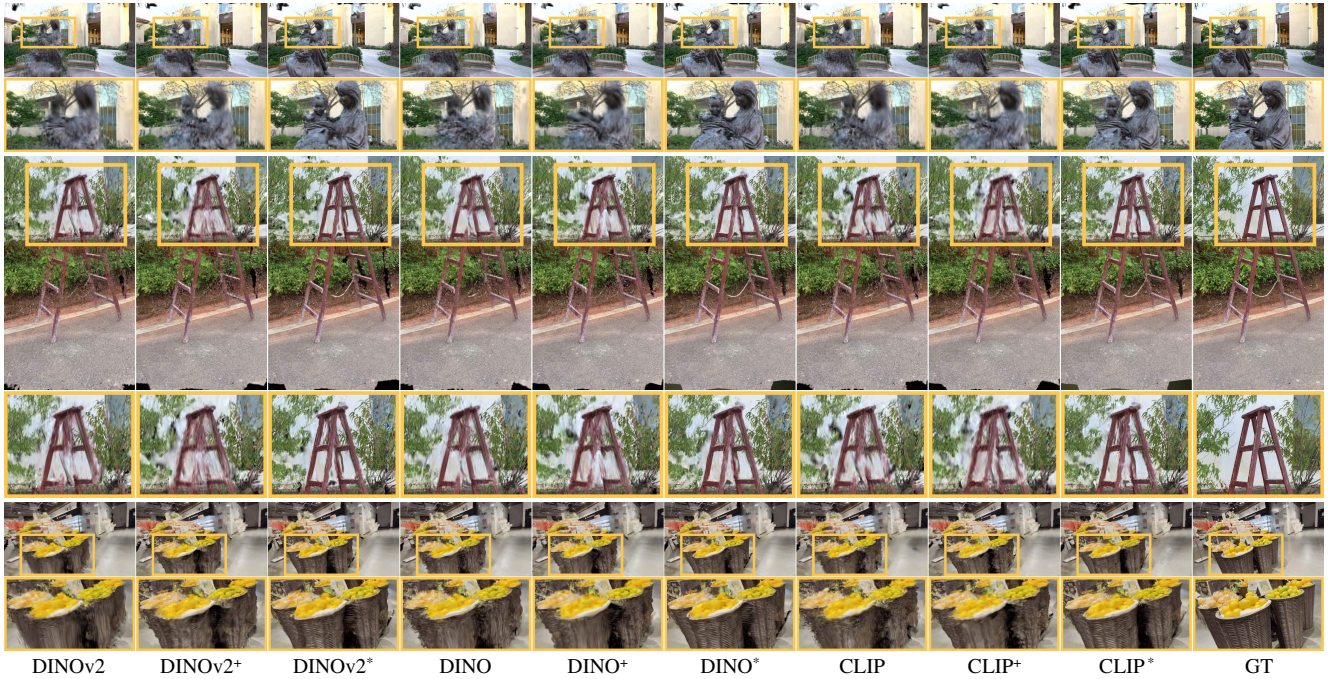


Figure R.3. **Feature Upsampling⁺ vs. Fine-tuning^{*}**. We compare Feat2GS application baselines between feature upsampling using the recent VFM feature upsampler [25] and feature fine-tuning during the warm-start stage. While feature upsampling improves the spatial resolution of features, feature fine-tuning provides greater details. Similar fine-tuning performance across different VFM features show that fine-tuning enriches embedded information, enabling high-quality reconstruction with any well-initialized features.

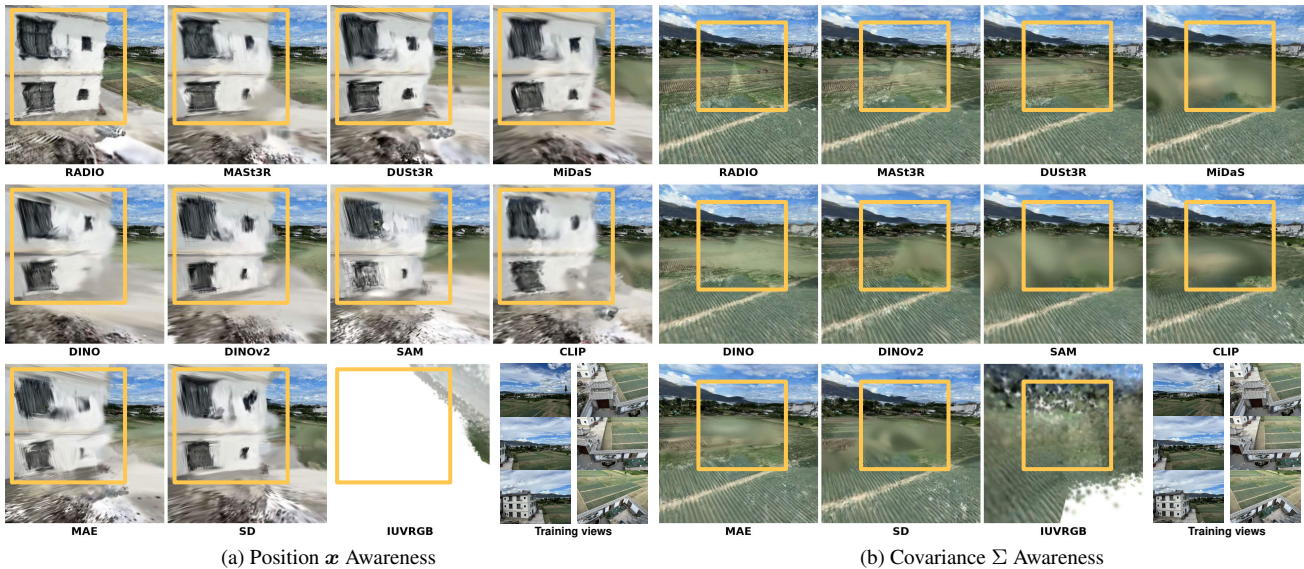


Figure R.4. **Two Geometry Awareness Attributes**. We illustrate different attributes of geometry awareness. Position x awareness is typically reflected in the sharpness of readout details and edges, while covariance Σ awareness is often observed in the flatness of planes.

Feature	LLFF									DL3DV									Casual								
	Geometry			Texture			All			Geometry			Texture			All			Geometry			Texture			All		
	PSNR \uparrow	SSIM \uparrow	LPIPS \downarrow	PSNR \uparrow	SSIM \uparrow	LPIPS \downarrow	PSNR \uparrow	SSIM \uparrow	LPIPS \downarrow	PSNR \uparrow	SSIM \uparrow	LPIPS \downarrow	PSNR \uparrow	SSIM \uparrow	LPIPS \downarrow	PSNR \uparrow	SSIM \uparrow	LPIPS \downarrow	PSNR \uparrow	SSIM \uparrow	LPIPS \downarrow	PSNR \uparrow	SSIM \uparrow	LPIPS \downarrow	PSNR \uparrow	SSIM \uparrow	LPIPS \downarrow
SD	19.62	.7293	.2234	18.85	.7100	.2297	19.78	.7121	.2656	19.31	.7251	.3276	17.79	.6784	.3260	19.10	.7282	.3500	19.24	.6483	.3649	17.38	.5698	.3789	18.86	.6505	.4053
Zero123	19.63	.7297	.2219	18.89	.7105	.2293	19.77	.7144	.2590	19.43	.7289	.3252	17.92	.6806	.3244	19.19	.7304	.3456	19.13	.6488	.3683	17.39	.5683	.3817	18.86	.6486	.4056
Feature	MipNeRF 360									MVImgNet									Tanks and Temples								
	Geometry			Texture			All			Geometry			Texture			All			Geometry			Texture			All		
	PSNR \uparrow	SSIM \uparrow	LPIPS \downarrow	PSNR \uparrow	SSIM \uparrow	LPIPS \downarrow	PSNR \uparrow	SSIM \uparrow	LPIPS \downarrow	PSNR \uparrow	SSIM \uparrow	LPIPS \downarrow	PSNR \uparrow	SSIM \uparrow	LPIPS \downarrow	PSNR \uparrow	SSIM \uparrow	LPIPS \downarrow	PSNR \uparrow	SSIM \uparrow	LPIPS \downarrow	PSNR \uparrow	SSIM \uparrow	LPIPS \downarrow	PSNR \uparrow	SSIM \uparrow	LPIPS \downarrow
SD	20.71	.4962	.3985	18.89	.4472	.3839	20.59	.4929	.4672	19.08	.5881	.3185	16.63	.5313	.3389	19.06	.5838	.3660	18.69	.6422	.3772	17.32	.6217	.3374	18.55	.6467	.4020
Zero123	20.74	.4942	.3966	19.07	.4520	.3817	20.72	.4953	.4599	19.05	.5842	.3253	16.75	.5332	.3376	19.09	.5873	.3588	18.50	.6376	.3806	17.59	.6241	.3363	18.34	.6409	.4011

Table R.2. **Zero123 vs. Stable Diffusion (SD)**. We report quantitative comparison between Zero123 and SD. It demonstrates that Zero123, which fine-tunes Stable Diffusion (SD) on Objaverse [19] multi-view dataset, captures geometry and texture better than SD in Objaverse-like simple scenes (LLFF) but performs worse in complex scenes (Tanks and Temples), which might be attributed to catastrophic forgetting [45].

	Fortress (LLFF)			Horns (LLFF)			Orchids (LLFF)			Room (LLFF)			Trex (LLFF)			Center (DL3DV)		
Feature	PSNR ↑	SSIM ↑	LPIPS ↓	PSNR ↑	SSIM ↑	LPIPS ↓	PSNR ↑	SSIM ↑	LPIPS ↓	PSNR ↑	SSIM ↑	LPIPS ↓	PSNR ↑	SSIM ↑	LPIPS ↓	PSNR ↑	SSIM ↑	LPIPS ↓
DUST3R	22.46	0.7766	0.1868	19.87	0.7428	0.1999	16.91	0.6095	0.2669	20.07	0.8339	0.2009	20.06	0.7580	0.2073	17.33	0.6510	0.3603
MAS3R	22.54	0.7854	0.1771	19.93	0.7402	0.2030	16.89	0.6063	0.2695	20.07	0.8341	0.1995	20.03	0.7576	0.2127	17.27	0.6479	0.3602
MiDaS	22.25	0.7811	0.1815	19.86	0.7326	0.2068	16.96	0.6106	0.2663	19.91	0.8259	0.2117	20.08	0.7599	0.2110	17.07	0.6411	0.3741
DINOV2	22.10	0.7514	0.2070	19.74	0.7232	0.2147	17.01	0.6084	0.2698	20.01	0.8303	0.2126	20.00	0.7593	0.2091	17.09	0.6446	0.3721
DINO	22.42	0.7743	0.1869	19.91	0.7435	0.1994	16.87	0.6071	0.2688	19.86	0.8298	0.2048	19.96	0.7570	0.2102	17.23	0.6451	0.3666
SAM	21.98	0.7572	0.2011	19.78	0.7234	0.2081	16.98	0.6083	0.2648	19.96	0.8286	0.2092	19.93	0.7596	0.2073	17.17	0.6446	0.3678
CLIP	22.47	0.7771	0.1907	19.83	0.7272	0.2153	16.86	0.6028	0.2761	19.89	0.8314	0.2121	19.83	0.7506	0.2164	17.17	0.6437	0.3777
RADIO	22.50	0.8017	0.1621	19.72	0.7314	0.2117	16.54	0.5911	0.2914	20.09	0.8325	0.2111	19.79	0.7442	0.2271	17.19	0.6448	0.3550
MAE	22.08	0.7577	0.2042	19.86	0.7234	0.2107	16.98	0.6107	0.2641	19.82	0.8320	0.2009	19.99	0.7579	0.2117	17.16	0.6438	0.3688
SD	21.62	0.7159	0.2280	19.86	0.7380	0.2047	16.78	0.6029	0.2722	19.84	0.8279	0.2039	19.98	0.7620	0.2084	17.19	0.6484	0.3648
IUVRGB	16.35	0.4913	0.4212	15.53	0.6048	0.3441	14.10	0.5086	0.4025	16.24	0.6920	0.4107	15.53	0.5858	0.4147	13.04	0.5478	0.4657
	Electrical (DL3DV)			Museum (DL3DV)			Supermarket2 (DL3DV)			Temple (DL3DV)			Erhai (Casual)			Paper2 (Casual)		
Feature	PSNR ↑	SSIM ↑	LPIPS ↓	PSNR ↑	SSIM ↑	LPIPS ↓	PSNR ↑	SSIM ↑	LPIPS ↓	PSNR ↑	SSIM ↑	LPIPS ↓	PSNR ↑	SSIM ↑	LPIPS ↓	PSNR ↑	SSIM ↑	LPIPS ↓
DUST3R	19.15	0.7566	0.3558	20.92	0.7853	0.2641	18.65	0.6855	0.3637	22.15	0.7906	0.2542	16.95	0.5876	0.3556	18.86	0.6313	0.3296
MAS3R	19.27	0.7579	0.3592	20.94	0.7823	0.2627	18.70	0.6893	0.3588	21.99	0.7896	0.2529	16.64	0.5698	0.3597	19.01	0.6336	0.3318
MiDaS	18.96	0.7496	0.3731	20.97	0.7828	0.2675	18.47	0.6739	0.3770	21.89	0.7880	0.2637	16.73	0.5848	0.3604	18.76	0.6355	0.3372
DINOV2	19.02	0.7520	0.3719	20.83	0.7862	0.2668	18.42	0.6749	0.3752	22.00	0.7889	0.2583	17.10	0.5804	0.3635	19.19	0.6310	0.3420
DINO	19.16	0.7563	0.3596	20.89	0.7834	0.2643	18.74	0.6871	0.3616	22.00	0.7901	0.2524	17.29	0.5681	0.3621	18.26	0.6298	0.3380
SAM	18.82	0.7484	0.3697	20.76	0.7835	0.2662	18.60	0.6796	0.3718	22.05	0.7926	0.2598	17.35	0.5670	0.3691	18.54	0.6279	0.3468
CLIP	19.14	0.7559	0.3717	20.90	0.7845	0.2695	18.43	0.6744	0.3777	22.02	0.7888	0.2556	17.15	0.5862	0.3685	18.16	0.6235	0.3498
RADIO	18.73	0.7499	0.3550	20.80	0.7774	0.2676	18.80	0.6943	0.3461	21.90	0.7902	0.2455	18.22	0.5840	0.3283	19.06	0.6369	0.3219
MAE	19.10	0.7543	0.3643	20.82	0.7808	0.2683	18.61	0.6762	0.3685	22.00	0.7890	0.2542	16.68	0.5783	0.3636	18.12	0.6229	0.3502
SD	18.30	0.7260	0.3812	20.64	0.7836	0.2684	18.59	0.6799	0.3646	21.81	0.7874	0.2591	17.81	0.5849	0.3550	18.40	0.6148	0.3413
IUVRGB	14.98	0.6666	0.4704	15.02	0.6545	0.4214	13.96	0.5839	0.5412	16.88	0.7101	0.3719	13.87	0.5076	0.4682	14.22	0.5846	0.4715
	Plushies (Casual)			Stuff (Casual)			Xbox (Casual)			Bicycle (MipNeRF 360)			Garden (MipNeRF 360)			Kitchen (MipNeRF 360)		
Feature	PSNR ↑	SSIM ↑	LPIPS ↓	PSNR ↑	SSIM ↑	LPIPS ↓	PSNR ↑	SSIM ↑	LPIPS ↓	PSNR ↑	SSIM ↑	LPIPS ↓	PSNR ↑	SSIM ↑	LPIPS ↓	PSNR ↑	SSIM ↑	LPIPS ↓
DUST3R	21.82	0.7282	0.3219	17.48	0.6726	0.3821	21.37	0.6614	0.4007	19.54	0.4024	0.4274	21.56	0.5254	0.3599	19.58	0.4907	0.3826
MAS3R	22.00	0.7323	0.3212	17.31	0.6753	0.3818	21.54	0.6640	0.3937	19.67	0.4073	0.4179	21.65	0.5356	0.3503	19.64	0.5002	0.3755
MiDaS	21.98	0.7278	0.3230	17.28	0.6659	0.3874	21.44	0.6587	0.3982	19.64	0.4066	0.4292	21.62	0.5260	0.3651	19.56	0.4983	0.3762
DINOV2	22.00	0.7298	0.3263	17.56	0.6717	0.3921	21.23	0.6493	0.4251	19.39	0.3942	0.4534	21.57	0.5139	0.3749	19.54	0.4767	0.3948
DINO	22.04	0.7302	0.3189	17.06	0.6694	0.3889	21.56	0.6590	0.3990	19.65	0.4085	0.4218	21.65	0.5264	0.3595	19.59	0.4922	0.3748
SAM	21.76	0.7229	0.3285	17.68	0.6668	0.3857	21.28	0.6497	0.4217	19.22	0.3874	0.4485	21.32	0.5011	0.3762	19.42	0.4780	0.3937
CLIP	21.72	0.7295	0.3333	17.34	0.6751	0.3930	21.69	0.6618	0.4150	19.61	0.4064	0.4460	21.44	0.5147	0.3713	19.48	0.4843	0.3854
RADIO	21.27	0.7185	0.3258	17.85	0.6743	0.3672	21.29	0.6587	0.3894	19.54	0.4058	0.4122	21.71	0.5458	0.3418	19.48	0.4987	0.3477
MAE	21.90	0.7260	0.3269	17.12	0.6687	0.3954	21.34	0.6550	0.4088	19.53	0.4042	0.4335	21.32	0.5105	0.3701	19.55	0.4905	0.3919
SD	21.61	0.7234	0.3262	17.25	0.6675	0.3831	21.13	0.6507	0.4190	19.44	0.4053	0.4593	21.48	0.5088	0.3790	19.31	0.4834	0.3965
IUVRGB	14.05	0.5294	0.5308	10.83	0.6095	0.5010	12.91	0.4959	0.6526	16.32	0.3683	0.6176	16.96	0.4022	0.5838	15.41	0.4142	0.5807
	Room (MipNeRF 360)			Stump (MipNeRF 360)			Bench (MipNeRF 360)			Bicycle (MipNeRF 360)			Car (MipNeRF 360)			Ladder (MipNeRF 360)		
Feature	PSNR ↑	SSIM ↑	LPIPS ↓	PSNR ↑	SSIM ↑	LPIPS ↓	PSNR ↑	SSIM ↑	LPIPS ↓	PSNR ↑	SSIM ↑	LPIPS ↓	PSNR ↑	SSIM ↑	LPIPS ↓	PSNR ↑	SSIM ↑	LPIPS ↓
DUST3R	23.50	0.7634	0.2501	19.90	0.3220	0.4773	18.28	0.4854	0.3376	17.23	0.4160	0.3982	22.18	0.8374	0.2063	18.26	0.5134	0.3325
MAS3R	23.55	0.7650	0.2519	20.09	0.3383	0.4770	18.30	0.4823	0.3302	17.25	0.4179	0.3895	22.24	0.8363	0.2019	18.23	0.5222	0.3287
MiDaS	23.62	0.7675	0.2509	20.02	0.3309	0.4860	18.02	0.4750	0.3597	17.01	0.4010	0.4111	22.15	0.8322	0.2134	18.32	0.5016	0.3405
DINOV2	23.54	0.7660	0.2597	20.01	0.3223	0.4937	18.31	0.4798	0.3600	17.07	0.3990	0.4170	22.03	0.8276	0.2181	18.11	0.4960	0.3425
DINO	23.66	0.7695	0.2462	20.03	0.3305	0.4822	18.31	0.4818	0.3399	17.11	0.4099	0.3952	22.12	0.8317	0.2095	18.38	0.5223	0.3286
SAM	23.76	0.7682	0.2620	19.92	0.3219	0.4920	18.19	0.4785	0.3493	17.01	0.4025	0.4078	21.64	0.8217	0.2215	18.10	0.5040	0.3393
CLIP	23.56	0.7669	0.2573	19.89	0.3187	0.4965	18.19	0.4866	0.3389	17.06	0.3988	0.4041	22.17	0.8356	0.2083	18.18	0.5064	0.3353
RADIO	23.67	0.7684	0.2380	19.94	0.3315	0.4703	18.20	0.4879	0.3247	17.20	0.4180	0.3895	22.65	0.8484	0.1901	18.36	0.5547	0.3193
MAE	23.70	0.7641	0.2561	20.00	0.3267	0.4903	18.17	0.4804	0.3391	16.97	0.4029	0.4004	21.66	0.8216	0.2221	18.14	0.5092	0.3364
SD	23.46	0.7598	0.2689	19.88	0.3239	0.4891	18.27	0.4818	0.3478	16.93	0.3964	0.4060	21.52	0.8277	0.2184	18.16	0.5015	0.3376
IUVRGB	17.05	0.5728	0.4828	16.54	0.2797	0.6903	14.32	0.4455	0.5308	12.89	0.2972	0.5970	17.53	0.7509	0.3281	17.13	0.4890	0.4393
	Suv (MipNeRF 360)			Auditorium (T&T)			Caterpillar (T&T)			Family (T&T)			Ignatius (T&T)			Train (T&T)		
Feature	PSNR ↑	SSIM ↑	LPIPS ↓	PSNR ↑	SSIM ↑	LPIPS ↓	PSNR ↑	SSIM ↑	LPIPS ↓	PSNR ↑	SSIM ↑	LPIPS ↓	PSNR ↑	SSIM ↑	LPIPS ↓	PSNR ↑	SSIM ↑	LPIPS ↓
DUST3R	21.39	0.7496	0.2617	19.87	0.7112	0.3684	18.78	0.5998	0.3820	19.61	0.6962	0.3223	18.21	0.6252	0.3604	17.76	0.5966	0.4243
MAS3R	21.42	0.7454	0.2659	19.68	0.7098	0.3658	18.72	0.5897	0.3813	19.68	0.6973	0.3195	18.01	0.6245	0.3630	17.93	0.5929	0.4220
MiDaS	21.27	0.7400	0.2864	19.92	0.7178	0.3647	18.45	0.5901	0.3978	19.35	0.6792	0.3320	18.05	0.6212	0.3642	16.90	0.5787	0.4405
DINOV2	21.24	0.7456	0.2852	19.89	0.7139	0.3668	18.78	0.6001	0.3847	19.38	0.6866	0.3306	17.94	0.6220	0.3698	17.56	0.5934	0.4341
DINO	21.30	0.7452	0.2623	19.91	0.7143	0.3650	18.78	0.5987	0.3822	19.34	0.6849	0.3272	18.22	0.6244	0.3602	17.48	0.5859	0.4319
SAM	21.22	0.7425	0.2759	19.99	0.7212	0.3616	18.60	0.5996	0.3889	19.38	0.6828	0.3284	18.11	0.6231	0.3611	17.17	0.5836	0.4501
CLIP	21.45	0.7452	0.2622	20.02	0.7149	0.3716	18.84	0.5975	0.3845	19.42	0.6885	0.3336	18.20	0.6241	0.3664	18.13	0.6064	0.4084
RADIO	21.32	0.7435	0.2509	20.00	0.7171	0.3588	19.05	0.6066	0.3639	19.80	0.7083	0.3028	18.27	0.6252	0.3473	18.84	0.6488	0.3674
MAE	21.22	0.7403	0.2730	20.11	0.7244	0.3595	18.35	0.5793	0.3918	19.32	0.6880	0.3257	18.19	0.6170	0.3598	17.30	0.5891	0.4420
SD	20.51	0.7330	0.2828	19.66	0.7074	0.3682	18.63	0.592										

	Fortress (LLFF)			Horns (LLFF)			Orchids (LLFF)			Room (LLFF)			Trex (LLFF)			Center (DL3DV)		
Feature	PSNR ↑	SSIM ↑	LPIPS ↓	PSNR ↑	SSIM ↑	LPIPS ↓	PSNR ↑	SSIM ↑	LPIPS ↓	PSNR ↑	SSIM ↑	LPIPS ↓	PSNR ↑	SSIM ↑	LPIPS ↓	PSNR ↑	SSIM ↑	LPIPS ↓
DUST3R	20.60	0.7404	0.2316	18.98	0.6957	0.1959	16.31	0.5814	0.2680	20.10	0.8135	0.2152	19.07	0.7291	0.2204	15.78	0.5908	0.3593
MAS3R	20.71	0.7439	0.2301	18.93	0.6934	0.1968	16.33	0.5807	0.2672	20.04	0.8118	0.2158	19.03	0.7278	0.2209	15.67	0.5854	0.3603
MiDaS	20.47	0.7430	0.2306	19.02	0.6965	0.1959	16.29	0.5800	0.2681	20.22	0.8161	0.2141	19.03	0.7290	0.2218	15.62	0.5827	0.3611
DINOV2	20.68	0.7438	0.2293	18.98	0.6960	0.1965	16.31	0.5817	0.2667	20.11	0.8149	0.2161	19.14	0.7300	0.2184	15.63	0.5828	0.3629
DINO	20.56	0.7431	0.2317	18.91	0.6938	0.1968	16.33	0.5805	0.2673	20.08	0.8138	0.2142	19.04	0.7290	0.2199	15.58	0.5805	0.3632
SAM	20.53	0.7449	0.2293	18.95	0.6964	0.1947	16.22	0.5800	0.2688	20.12	0.8152	0.2148	19.08	0.7298	0.2227	15.44	0.5848	0.3594
CLIP	20.79	0.7444	0.2306	18.90	0.6941	0.1970	16.35	0.5810	0.2675	19.97	0.8088	0.2214	19.09	0.7282	0.2217	15.80	0.5838	0.3614
RADIO	21.07	0.7442	0.2320	18.88	0.6929	0.1982	16.35	0.5806	0.2700	19.82	0.8030	0.2289	19.18	0.7298	0.2215	15.91	0.5822	0.3636
MAE	20.52	0.7405	0.2300	18.99	0.6974	0.1959	16.30	0.5805	0.2684	20.06	0.8144	0.2122	19.16	0.7313	0.2182	15.59	0.5852	0.3600
SD	20.18	0.7377	0.2325	18.93	0.6945	0.1978	16.18	0.5774	0.2719	20.03	0.8132	0.2206	18.95	0.7270	0.2258	15.58	0.5879	0.3617
IUVRGB	22.01	0.7543	0.2290	19.39	0.7170	0.2114	16.75	0.5997	0.2630	20.79	0.8323	0.2060	19.79	0.7482	0.2215	16.59	0.6108	0.3719
	Electrical (DL3DV)			Museum (DL3DV)			Supermarket2 (DL3DV)			Temple (DL3DV)			Erhai (Casual)			Paper2 (Casual)		
Feature	PSNR ↑	SSIM ↑	LPIPS ↓	PSNR ↑	SSIM ↑	LPIPS ↓	PSNR ↑	SSIM ↑	LPIPS ↓	PSNR ↑	SSIM ↑	LPIPS ↓	PSNR ↑	SSIM ↑	LPIPS ↓	PSNR ↑	SSIM ↑	LPIPS ↓
DUST3R	17.17	0.6887	0.3678	18.77	0.7214	0.2988	17.62	0.6537	0.3315	20.69	0.7528	0.2520	17.29	0.5748	0.3260	16.15	0.5327	0.3849
MAS3R	17.19	0.6892	0.3644	18.97	0.7250	0.2972	17.65	0.6542	0.3318	20.85	0.7527	0.2520	17.36	0.5752	0.3250	16.27	0.5358	0.3794
MiDaS	17.05	0.6891	0.3671	18.79	0.7204	0.2984	17.65	0.6537	0.3324	20.60	0.7520	0.2528	17.26	0.5750	0.3264	16.07	0.5301	0.3840
DINOV2	17.03	0.6894	0.3679	18.93	0.7244	0.2973	17.68	0.6525	0.3315	20.75	0.7537	0.2520	17.32	0.5746	0.3270	16.57	0.5333	0.3852
DINO	17.07	0.6846	0.3676	18.81	0.7230	0.2966	17.63	0.6557	0.3303	20.78	0.7515	0.2519	17.26	0.5735	0.3268	16.24	0.5345	0.3827
SAM	17.21	0.6905	0.3698	18.85	0.7255	0.2975	17.69	0.6557	0.3308	20.65	0.7547	0.2513	17.25	0.5716	0.3274	16.26	0.5403	0.3815
CLIP	17.16	0.6796	0.3695	18.86	0.7188	0.3012	17.63	0.6541	0.3297	20.79	0.7492	0.2557	17.23	0.5730	0.3258	16.04	0.5327	0.3834
RADIO	17.09	0.6767	0.3707	18.75	0.7161	0.3020	17.52	0.6503	0.3342	20.88	0.7486	0.2564	17.22	0.5725	0.3264	16.25	0.5360	0.3801
MAE	17.07	0.6913	0.3651	18.76	0.7227	0.2974	17.75	0.6578	0.3294	20.72	0.7536	0.2516	17.29	0.5648	0.3301	16.16	0.5372	0.3820
SD	16.63	0.6804	0.3748	18.67	0.7191	0.3045	17.56	0.6526	0.3341	20.50	0.7521	0.2550	17.39	0.5729	0.3278	15.94	0.5354	0.3909
IUVRGB	17.77	0.7065	0.3711	19.71	0.7490	0.2889	18.16	0.6746	0.3336	21.51	0.7708	0.2595	17.27	0.5748	0.3416	16.98	0.5549	0.3865
	Plushies (Casual)			Stuff (Casual)			Xbox (Casual)			Bicycle (MipNeRF 360)			Garden (MipNeRF 360)			Kitchen (MipNeRF 360)		
Feature	PSNR ↑	SSIM ↑	LPIPS ↓	PSNR ↑	SSIM ↑	LPIPS ↓	PSNR ↑	SSIM ↑	LPIPS ↓	PSNR ↑	SSIM ↑	LPIPS ↓	PSNR ↑	SSIM ↑	LPIPS ↓	PSNR ↑	SSIM ↑	LPIPS ↓
DUST3R	19.13	0.6324	0.3284	15.84	0.5362	0.4095	19.28	0.5705	0.4262	17.02	0.3276	0.4265	19.91	0.4838	0.3576	17.94	0.4203	0.3733
MAS3R	19.06	0.6311	0.3280	16.08	0.5398	0.4028	19.18	0.5720	0.4255	17.18	0.3295	0.4252	19.87	0.4851	0.3563	18.22	0.4441	0.3716
MiDaS	19.01	0.6301	0.3295	15.87	0.5383	0.4141	19.39	0.5730	0.4242	16.90	0.3270	0.4278	19.93	0.4876	0.3568	18.02	0.4340	0.3707
DINOV2	18.97	0.6285	0.3324	16.02	0.5426	0.4061	19.32	0.5718	0.4266	17.08	0.3279	0.4277	19.93	0.4866	0.3535	17.93	0.4271	0.3774
DINO	18.99	0.6304	0.3300	15.77	0.5331	0.4089	19.25	0.5700	0.4299	16.98	0.3263	0.4276	19.93	0.4837	0.3558	18.28	0.4538	0.3651
SAM	18.95	0.6308	0.3308	16.02	0.5500	0.4032	19.09	0.5696	0.4249	17.14	0.3311	0.4239	19.96	0.4865	0.3524	18.17	0.4543	0.3623
CLIP	18.92	0.6273	0.3310	15.85	0.5300	0.4050	19.27	0.5717	0.4261	17.26	0.3350	0.4255	19.94	0.4828	0.3582	18.27	0.4408	0.3688
RADIO	19.08	0.6271	0.3320	15.75	0.5262	0.4088	19.31	0.5710	0.4267	17.34	0.3358	0.4249	19.88	0.4822	0.3629	18.36	0.4371	0.3719
MAE	18.98	0.6317	0.3297	15.95	0.5411	0.4115	19.15	0.5707	0.4260	17.14	0.3289	0.4255	19.92	0.4868	0.3533	18.22	0.4635	0.3611
SD	18.63	0.6275	0.3356	15.92	0.5467	0.4102	19.00	0.5667	0.4301	16.95	0.3308	0.4274	19.91	0.4852	0.3545	17.74	0.4231	0.3791
IUVRGB	19.06	0.6423	0.3558	16.48	0.5811	0.4043	19.59	0.6103	0.4350	18.21	0.3644	0.4312	20.59	0.5079	0.3743	18.93	0.4692	0.3751
	Room (MipNeRF 360)			Stump (MipNeRF 360)			Bench (MipNeRF 360)			Bicycle (MipNeRF 360)			Car (MipNeRF 360)			Ladder (MipNeRF 360)		
Feature	PSNR ↑	SSIM ↑	LPIPS ↓	PSNR ↑	SSIM ↑	LPIPS ↓	PSNR ↑	SSIM ↑	LPIPS ↓	PSNR ↑	SSIM ↑	LPIPS ↓	PSNR ↑	SSIM ↑	LPIPS ↓	PSNR ↑	SSIM ↑	LPIPS ↓
DUST3R	22.47	0.7343	0.2611	18.16	0.2785	0.4895	15.72	0.4193	0.3685	14.46	0.3379	0.4314	20.22	0.7926	0.2277	16.20	0.4866	0.3314
MAS3R	22.55	0.7315	0.2611	18.22	0.2800	0.4875	15.68	0.4197	0.3695	14.52	0.3381	0.4306	20.21	0.7894	0.2303	16.31	0.4874	0.3298
MiDaS	22.36	0.7303	0.2629	18.05	0.2757	0.4881	15.64	0.4198	0.3706	14.47	0.3374	0.4304	20.07	0.7901	0.2299	16.17	0.4832	0.3327
DINOV2	22.13	0.7282	0.2638	18.20	0.2778	0.4883	15.65	0.4198	0.3702	14.47	0.3376	0.4311	20.17	0.7908	0.2308	16.17	0.4872	0.3313
DINO	22.48	0.7305	0.2617	18.21	0.2782	0.4873	15.70	0.4192	0.3712	14.39	0.3361	0.4323	20.15	0.7899	0.2287	16.35	0.5073	0.3250
SAM	22.28	0.7292	0.2630	18.12	0.2772	0.4860	15.67	0.4229	0.3691	14.44	0.3359	0.4330	20.09	0.7878	0.2323	16.25	0.4893	0.3297
CLIP	22.59	0.7354	0.2617	18.35	0.2774	0.4893	15.66	0.4200	0.3719	14.52	0.3377	0.4332	20.04	0.7880	0.2325	16.36	0.4965	0.3278
RADIO	22.59	0.7361	0.2620	18.58	0.2840	0.4877	15.64	0.4188	0.3715	14.50	0.3384	0.4324	20.32	0.7874	0.2345	16.44	0.5082	0.3268
MAE	22.26	0.7284	0.2641	18.17	0.2786	0.4867	15.70	0.4183	0.3703	14.47	0.3380	0.4299	20.02	0.7910	0.2291	16.17	0.4879	0.3300
SD	21.99	0.7216	0.2699	17.84	0.2754	0.4885	15.51	0.4209	0.3752	14.30	0.3336	0.4358	19.90	0.7911	0.2320	16.11	0.4875	0.3319
IUVRGB	23.14	0.7507	0.2660	18.96	0.3064	0.5091	16.49	0.4480	0.3764	15.10	0.3640	0.4509	20.68	0.7946	0.2389	17.15	0.5289	0.3403
	Suv (MipNeRF 360)			Auditorium (T&T)			Caterpillar (T&T)			Family (T&T)			Ignatius (T&T)			Train (T&T)		
Feature	PSNR ↑	SSIM ↑	LPIPS ↓	PSNR ↑	SSIM ↑	LPIPS ↓	PSNR ↑	SSIM ↑	LPIPS ↓	PSNR ↑	SSIM ↑	LPIPS ↓	PSNR ↑	SSIM ↑	LPIPS ↓	PSNR ↑	SSIM ↑	LPIPS ↓
DUST3R	17.77	0.6377	0.3081	17.92	0.6637	0.3595	16.39	0.5543	0.3552	19.64	0.6914	0.2650	16.54	0.5722	0.3542	17.14	0.6294	0.3303
MAS3R	17.80	0.6402	0.3084	18.11	0.6667	0.3573	17.05	0.5632	0.3533	19.52	0.6884	0.2671	16.70	0.5732	0.3522	16.99	0.6273	0.3295
MiDaS	17.73	0.6378	0.3081	17.97	0.6623	0.3624	17.14	0.5676	0.3527	19.49	0.6896	0.2659	16.50	0.5707	0.3566	17.12	0.6288	0.3288
DINOV2	17.94	0.6442	0.3085	17.58	0.6503	0.3684	17.21	0.5693	0.3521	19.43	0.6883	0.2685	16.68	0.5710	0.3549	16.98	0.6284	0.3299
DINO	17.92	0.6446	0.3073	18.03	0.6634	0.3623	17.17	0.5673	0.3528	19.51	0.6866	0.2677	16.63	0.5721	0.3530	16.96	0.6274	0.3292
SAM	17.74	0.6370	0.3087	17.57	0.6523	0.3671	16.83	0.5636	0.3541	19.41	0.6899	0.2662	16.55	0.5714	0.3549	17.11	0.6312	0.3265
CLIP	18.22	0.6386	0.3135	17.96	0.6600	0.3619	17.42	0.5664	0.3511	19.69	0.6893	0.2655	16.79	0.5708	0.3537	17.19	0.6264	0.3256
RADIO	18.04	0.6339	0.3178	18.14	0.6636	0.3591	17.58	0.5676	0.3514	19.60	0.6883	0.2683	16.81	0.5707	0.3539	17.06	0.6224	0.3278
MAE	17.85	0.6425	0.3048	17.98	0.6649	0.3591	17.00	0.5647	0.3539	19.43	0.6890	0.2675	16.36	0.5702	0.3547	16.97	0.6283	0.3313
SD	17.36	0.6232	0.3197	18.11	0.6675	0.3629	15.84	0.548										

	Fortress (LLFF)			Horns (LLFF)			Orchids (LLFF)			Room (LLFF)			Trex (LLFF)			Center (DL3DV)		
Feature	PSNR ↑	SSIM ↑	LPIPS ↓	PSNR ↑	SSIM ↑	LPIPS ↓	PSNR ↑	SSIM ↑	LPIPS ↓	PSNR ↑	SSIM ↑	LPIPS ↓	PSNR ↑	SSIM ↑	LPIPS ↓	PSNR ↑	SSIM ↑	LPIPS ↓
DUST3R	21.94	0.6621	0.3051	20.14	0.7186	0.2790	17.25	0.6290	0.2838	19.99	0.8304	0.2361	20.04	0.7551	0.2417	16.85	0.6532	0.3773
MAS3R	22.26	0.6833	0.2845	20.08	0.7204	0.2816	17.36	0.6358	0.2792	20.07	0.8292	0.2380	20.20	0.7565	0.2453	16.91	0.6539	0.3769
MiDaS	21.66	0.6357	0.3207	20.16	0.7164	0.2817	17.14	0.6302	0.2832	20.33	0.8323	0.2380	20.01	0.7563	0.2428	16.56	0.6365	0.3888
DINOV2	21.74	0.6465	0.2852	20.03	0.7173	0.2758	17.13	0.6282	0.2836	20.47	0.8308	0.2362	20.19	0.7588	0.2376	16.40	0.6394	0.3840
DINO	22.17	0.6668	0.3114	20.10	0.7192	0.2804	17.22	0.6329	0.2847	20.28	0.8307	0.2466	20.11	0.7563	0.2488	16.84	0.6534	0.3830
SAM	21.24	0.6282	0.3141	19.85	0.7177	0.2706	17.21	0.6292	0.2726	20.42	0.8362	0.2221	20.08	0.7605	0.2352	16.39	0.6315	0.3884
CLIP	22.11	0.6604	0.2920	19.95	0.7123	0.2942	17.19	0.6282	0.2983	19.40	0.8181	0.2628	20.06	0.7488	0.2638	16.89	0.6494	0.3909
RADIO	21.67	0.6282	0.3893	19.78	0.7003	0.3185	17.07	0.6196	0.3381	19.09	0.8118	0.2814	20.19	0.7395	0.2988	16.96	0.6614	0.3884
MAE	21.78	0.6612	0.2949	20.25	0.7220	0.2744	17.21	0.6287	0.2786	20.22	0.8324	0.2262	20.14	0.7602	0.2320	16.56	0.6261	0.3896
SD	21.51	0.6272	0.3051	19.89	0.7192	0.2626	17.16	0.6279	0.2797	20.23	0.8278	0.2403	20.10	0.7585	0.2404	16.73	0.6463	0.3829
IUVRGB	18.11	0.5288	0.5189	14.73	0.6269	0.3682	13.62	0.5686	0.4688	15.78	0.7217	0.4118	14.66	0.6415	0.3866	13.45	0.5626	0.4564
	Electrical (DL3DV)			Museum (DL3DV)			Supermarket2 (DL3DV)			Temple (DL3DV)			Erhai (Casual)			Paper2 (Casual)		
Feature	PSNR ↑	SSIM ↑	LPIPS ↓	PSNR ↑	SSIM ↑	LPIPS ↓	PSNR ↑	SSIM ↑	LPIPS ↓	PSNR ↑	SSIM ↑	LPIPS ↓	PSNR ↑	SSIM ↑	LPIPS ↓	PSNR ↑	SSIM ↑	LPIPS ↓
DUST3R	18.90	0.7615	0.3775	20.81	0.7906	0.2842	18.44	0.6800	0.3973	21.93	0.7945	0.2925	17.35	0.5822	0.4179	18.28	0.6528	0.3832
MAS3R	19.11	0.7680	0.3753	20.63	0.7902	0.2857	18.50	0.6795	0.4009	21.90	0.7950	0.2932	17.72	0.5873	0.4160	18.83	0.6559	0.3770
MiDaS	18.75	0.7570	0.3804	20.80	0.7900	0.2823	18.22	0.6716	0.4021	21.77	0.7904	0.2931	16.81	0.5824	0.4115	18.48	0.6528	0.3804
DINOV2	19.14	0.7657	0.3791	20.71	0.7903	0.2842	18.33	0.6734	0.4003	21.77	0.7897	0.2920	16.83	0.5802	0.4119	19.19	0.6584	0.3668
DINO	19.01	0.7626	0.3764	20.76	0.7905	0.2871	18.46	0.6786	0.4000	21.99	0.7943	0.2916	17.72	0.5873	0.4172	18.27	0.6537	0.3719
SAM	18.72	0.7501	0.3775	20.52	0.7877	0.2813	18.42	0.6729	0.3944	21.96	0.7939	0.2879	16.65	0.5789	0.4089	19.14	0.6530	0.3744
CLIP	18.48	0.7529	0.3919	20.66	0.7894	0.2906	18.18	0.6707	0.4121	21.89	0.7924	0.2958	16.45	0.5849	0.4202	18.84	0.6613	0.3774
RADIO	18.74	0.7611	0.3968	20.37	0.7751	0.3036	18.13	0.6712	0.4243	21.78	0.7890	0.3139	16.57	0.5875	0.4243	18.37	0.6603	0.3811
MAE	19.04	0.7639	0.3764	20.73	0.7903	0.2783	18.39	0.6792	0.3923	22.00	0.7956	0.2874	17.30	0.5776	0.4087	18.86	0.6552	0.3740
SD	18.20	0.7431	0.3870	20.50	0.7821	0.2907	18.46	0.6781	0.3970	21.60	0.7915	0.2924	16.65	0.5803	0.4089	18.96	0.6510	0.3751
IUVRGB	12.68	0.6689	0.4550	13.86	0.6614	0.4159	13.51	0.5942	0.5106	16.76	0.7283	0.3550	16.00	0.5691	0.4759	14.07	0.6253	0.4337
	Plushies (Casual)			Stuff (Casual)			Xbox (Casual)			Bicycle (MipNeRF 360)			Garden (MipNeRF 360)			Kitchen (MipNeRF 360)		
Feature	PSNR ↑	SSIM ↑	LPIPS ↓	PSNR ↑	SSIM ↑	LPIPS ↓	PSNR ↑	SSIM ↑	LPIPS ↓	PSNR ↑	SSIM ↑	LPIPS ↓	PSNR ↑	SSIM ↑	LPIPS ↓	PSNR ↑	SSIM ↑	LPIPS ↓
DUST3R	21.89	0.6947	0.3858	17.62	0.6893	0.3806	20.82	0.6588	0.4574	19.82	0.4221	0.5193	21.80	0.4866	0.4971	19.59	0.5070	0.4570
MAS3R	21.81	0.6939	0.3890	17.54	0.6946	0.3752	20.94	0.6626	0.4566	19.91	0.4245	0.5253	21.73	0.4877	0.5002	19.41	0.5031	0.4437
MiDaS	21.71	0.6863	0.3926	17.26	0.6855	0.3882	20.52	0.6512	0.4639	19.96	0.4248	0.5262	21.52	0.4812	0.5029	19.51	0.4983	0.4639
DINOV2	21.34	0.6882	0.3813	17.83	0.6893	0.3844	20.85	0.6514	0.4669	19.47	0.4063	0.5162	21.56	0.4804	0.4960	19.49	0.4882	0.4469
DINO	21.68	0.6916	0.3868	17.02	0.6898	0.3980	20.81	0.6604	0.4539	19.91	0.4208	0.5250	21.52	0.4825	0.4978	19.02	0.4900	0.4609
SAM	21.63	0.7028	0.3692	17.87	0.6945	0.3820	20.67	0.6553	0.4559	19.34	0.4083	0.5180	21.56	0.4815	0.4815	19.28	0.4956	0.4445
CLIP	21.51	0.6901	0.3939	17.27	0.6911	0.3870	21.16	0.6634	0.4635	19.96	0.4220	0.5310	21.61	0.4795	0.5063	19.13	0.4795	0.4465
RADIO	21.04	0.6726	0.4358	16.67	0.6952	0.3792	20.73	0.6507	0.4876	20.11	0.4320	0.5567	21.57	0.4752	0.5379	19.68	0.5119	0.4842
MAE	21.35	0.6909	0.3719	17.67	0.6893	0.3819	20.74	0.6604	0.4503	19.66	0.4159	0.5175	21.63	0.4843	0.4889	19.18	0.4928	0.4490
SD	21.22	0.6882	0.3793	17.06	0.6813	0.4009	20.41	0.6517	0.4625	19.53	0.4129	0.5117	21.63	0.4828	0.4832	19.04	0.4843	0.4431
IUVRGB	13.13	0.5682	0.5347	13.18	0.6617	0.4288	12.18	0.5344	0.6042	16.20	0.6214	0.6213	17.34	0.4313	0.5962	15.02	0.4498	0.5853
	Room (MipNeRF 360)			Stump (MipNeRF 360)			Bench (MipNeRF 360)			Bicycle (MipNeRF 360)			Car (MipNeRF 360)			Ladder (MipNeRF 360)		
Feature	PSNR ↑	SSIM ↑	LPIPS ↓	PSNR ↑	SSIM ↑	LPIPS ↓	PSNR ↑	SSIM ↑	LPIPS ↓	PSNR ↑	SSIM ↑	LPIPS ↓	PSNR ↑	SSIM ↑	LPIPS ↓	PSNR ↑	SSIM ↑	LPIPS ↓
DUST3R	23.72	0.7591	0.3261	20.16	0.3491	0.5767	19.05	0.5092	0.4156	17.29	0.3711	0.4937	21.78	0.8338	0.2357	18.47	0.5120	0.3875
MAS3R	23.42	0.7623	0.3256	20.14	0.3493	0.5798	19.09	0.5125	0.4078	17.23	0.3677	0.4961	21.68	0.8372	0.2313	18.42	0.5118	0.3870
MiDaS	23.19	0.7548	0.3334	20.02	0.3428	0.5709	18.71	0.5031	0.4101	17.20	0.3692	0.4970	21.46	0.8270	0.2372	18.44	0.5088	0.3844
DINOV2	23.32	0.7543	0.3262	19.89	0.3326	0.5566	18.71	0.4976	0.4137	17.14	0.3669	0.4981	21.55	0.8327	0.2370	18.57	0.5121	0.3837
DINO	23.56	0.7639	0.3259	20.12	0.3478	0.5766	18.91	0.5079	0.4102	17.22	0.3665	0.5039	21.84	0.8384	0.2280	18.58	0.5112	0.3898
SAM	23.70	0.7551	0.3219	19.87	0.3338	0.5539	18.76	0.5040	0.4059	17.15	0.3655	0.4971	21.25	0.8267	0.2348	18.44	0.5077	0.3839
CLIP	23.59	0.7690	0.3314	20.12	0.3422	0.5715	18.94	0.5122	0.4139	17.29	0.3727	0.5013	21.75	0.8366	0.2331	18.44	0.5123	0.3900
RADIO	22.87	0.7567	0.3532	20.32	0.3575	0.6313	19.17	0.5069	0.4558	17.44	0.3574	0.5426	21.64	0.8341	0.2505	18.79	0.5233	0.4130
MAE	23.37	0.7638	0.3206	20.10	0.3405	0.5582	18.77	0.5038	0.4136	17.24	0.3670	0.5017	21.55	0.8307	0.2352	18.12	0.5054	0.3887
SD	22.90	0.7455	0.3308	19.84	0.3388	0.5672	18.34	0.4888	0.4103	16.87	0.3628	0.4984	21.65	0.8324	0.2337	18.30	0.5075	0.3760
IUVRGB	14.55	0.5198	0.5069	18.96	0.3311	0.6547	15.69	0.4710	0.5220	13.80	0.2845	0.6120	15.41	0.7494	0.3134	17.20	0.5072	0.4651
	Suv (MipNeRF 360)			Auditorium (T&T)			Caterpillar (T&T)			Family (T&T)			Ignatius (T&T)			Train (T&T)		
Feature	PSNR ↑	SSIM ↑	LPIPS ↓	PSNR ↑	SSIM ↑	LPIPS ↓	PSNR ↑	SSIM ↑	LPIPS ↓	PSNR ↑	SSIM ↑	LPIPS ↓	PSNR ↑	SSIM ↑	LPIPS ↓	PSNR ↑	SSIM ↑	LPIPS ↓
DUST3R	20.54	0.7425	0.3046	19.19	0.7052	0.3851	18.98	0.6161	0.4151	19.15	0.6845	0.3690	18.48	0.6409	0.3950	17.22	0.5917	0.4472
MAS3R	21.04	0.7623	0.2965	19.62	0.7155	0.3750	18.94	0.6190	0.4141	19.20	0.6853	0.3694	18.50	0.6402	0.3934	17.55	0.5962	0.4439
MiDaS	20.90	0.7467	0.3074	19.45	0.7156	0.3813	17.96	0.5952	0.4199	18.91	0.6795	0.3700	18.28	0.6321	0.3899	16.97	0.5918	0.4584
DINOV2	21.18	0.7623	0.3047	19.78	0.7176	0.3766	18.52	0.6052	0.4216	18.77	0.6783	0.3725	18.14	0.6344	0.3987	16.96	0.5862	0.4626
DINO	20.51	0.7518	0.3095	19.64	0.7163	0.3817	18.91	0.6121	0.4161	18.98	0.6813	0.3701	18.27	0.6348	0.3948	17.23	0.5888	0.4522
SAM	20.84	0.7537	0.3027	19.62	0.7151	0.3790	18.77	0.6045	0.4118	19.02	0.6803	0.3681	18.03	0.6325	0.3904	16.71	0.5799	0.4653
CLIP	20.45	0.7505	0.3090	19.82	0.7169	0.3857	18.66	0.6124	0.4241	19.27	0.6821	0.3777	18.32	0.6371	0.4034	17.70	0.6091	0.4352
RADIO	20.97	0.7558	0.3112	19.53	0.7131	0.3928	18.96	0.6225	0.4293	19.58	0.6879	0.3879	18.65	0.6416	0.4070	18.33	0.6219	0.4377
MAE	20.55	0.7500	0.3010	19.55	0.7120	0.3785	18.77	0.6110	0.4091	19.19	0.6833	0.3648	18.03	0.6324	0.3912	16.91	0.5869	0.4563
SD	20.11	0.7276	0.3118	19.11	0.7053	0.3867	18.78	0.608										

Feature	Scan1 (DTU)						Scan23 (DTU)						Scan4 (DTU)						Scan75 (DTU)					
	PSNR ↑	SSIM ↑	LPIPS ↓	Acc. ↓	Comp. ↓	Dist. ↓	PSNR ↑	SSIM ↑	LPIPS ↓	Acc. ↓	Comp. ↓	Dist. ↓	PSNR ↑	SSIM ↑	LPIPS ↓	Acc. ↓	Comp. ↓	Dist. ↓	PSNR ↑	SSIM ↑	LPIPS ↓	Acc. ↓	Comp. ↓	Dist. ↓
DUS3R	22.19	0.7604	0.2374	2.042	1.267	7.569	19.64	0.6427	0.3100	1.781	1.374	6.130	19.28	0.6618	0.2554	2.848	1.515	7.165	23.52	0.8240	0.1652	3.101	1.434	8.311
MAS3R	22.22	0.7649	0.2334	1.876	1.139	6.645	19.45	0.6393	0.3128	1.808	1.380	6.066	19.44	0.6680	0.2513	2.708	1.478	6.756	23.23	0.8260	0.1641	3.056	1.499	7.968
MiDaS	22.08	0.7559	0.2441	2.602	1.394	8.196	19.50	0.6334	0.3170	2.326	1.542	7.626	19.44	0.6676	0.2539	3.140	1.588	7.899	23.33	0.8219	0.1679	3.345	1.461	8.839
DINov2	21.58	0.7481	0.2552	3.722	1.359	11.194	19.04	0.6259	0.3200	2.374	1.355	7.773	19.10	0.6558	0.2627	3.298	1.440	8.520	23.30	0.8251	0.1688	3.926	1.571	9.425
DINO	21.91	0.7554	0.2430	2.411	1.328	7.721	19.36	0.6379	0.3145	1.975	1.432	6.407	19.25	0.6641	0.2510	2.775	1.493	6.821	23.36	0.8280	0.1634	3.325	1.612	8.259
SAM	21.76	0.7492	0.2536	3.128	1.329	9.381	19.00	0.6176	0.3254	2.678	1.291	9.178	19.14	0.6600	0.2627	3.335	1.532	8.396	23.32	0.8187	0.1724	3.820	1.456	9.740
CLIP	21.79	0.7498	0.2472	2.262	1.137	7.294	19.32	0.6333	0.3198	1.914	1.373	6.195	19.32	0.6643	0.2540	2.694	1.373	7.094	23.33	0.8260	0.1653	2.977	1.387	7.748
RADIO	22.61	0.7774	0.2148	1.241	1.073	5.328	19.31	0.6409	0.3037	1.702	1.570	5.273	19.69	0.6739	0.2388	2.439	1.686	6.287	23.79	0.8527	0.1477	2.697	1.641	6.882
MAE	21.71	0.7476	0.2541	3.256	1.351	10.750	19.01	0.6229	0.3208	2.244	1.407	7.539	19.07	0.6576	0.2646	3.203	1.461	8.163	23.43	0.8216	0.1681	3.436	1.417	8.689
SD	21.28	0.7434	0.2606	5.212	1.649	13.766	19.07	0.6208	0.3278	3.453	1.564	11.532	18.84	0.6519	0.2690	4.431	1.754	10.571	23.41	0.8199	0.1725	5.334	1.878	12.456
IUVRGB	16.24	0.6967	0.3243	16.673	23.935	38.901	14.01	0.4927	0.4406	16.833	13.469	73.607	12.64	0.5816	0.3750	15.078	20.257	69.307	19.63	0.7977	0.2143	12.262	15.690	40.133
Scan9 (DTU)																								
Feature	PSNR ↑	SSIM ↑	LPIPS ↓	Acc. ↓	Comp. ↓	Dist. ↓	PSNR ↑	SSIM ↑	LPIPS ↓	Acc. ↓	Comp. ↓	Dist. ↓	PSNR ↑	SSIM ↑	LPIPS ↓	Acc. ↓	Comp. ↓	Dist. ↓	PSNR ↑	SSIM ↑	LPIPS ↓	Acc. ↓	Comp. ↓	Dist. ↓
DUS3R	19.29	0.6866	0.3106	1.860	1.140	5.944	20.53	0.7889	0.2103	2.090	1.244	6.577	21.94	0.8048	0.2495	2.304	1.094	7.266	24.76	0.8767	0.1442	2.299	1.181	6.556
MAS3R	19.38	0.6878	0.3092	1.680	1.088	5.285	20.44	0.7876	0.2117	2.103	1.242	6.230	21.68	0.8022	0.2552	2.110	1.090	6.237	24.83	0.8776	0.1431	2.209	1.235	6.413
MiDaS	19.44	0.6759	0.3179	2.412	1.200	7.370	19.78	0.7709	0.2256	3.824	1.550	10.567	21.68	0.8020	0.2488	2.770	1.160	8.400	24.12	0.8716	0.1478	2.487	1.277	7.158
DINov2	19.33	0.6791	0.3153	2.191	1.147	7.162	20.00	0.7733	0.2248	3.476	1.462	8.763	21.50	0.8039	0.2535	2.990	1.125	9.059	24.61	0.8745	0.1468	2.456	1.154	7.260
DINO	19.83	0.6904	0.3074	1.770	1.098	5.542	20.38	0.7876	0.2109	2.362	1.211	7.103	21.83	0.8019	0.2498	2.370	1.126	7.559	24.45	0.8758	0.1440	2.006	1.172	5.859
SAM	19.11	0.6650	0.3252	2.495	1.110	8.064	19.99	0.7774	0.2224	3.307	1.478	8.919	21.14	0.7897	0.2618	3.084	1.175	9.145	24.67	0.8732	0.1468	2.560	1.176	7.627
CLIP	19.33	0.6835	0.3158	1.596	1.009	5.203	20.26	0.7769	0.2193	2.338	1.180	6.781	21.76	0.8032	0.2575	2.244	1.027	7.124	24.54	0.8747	0.1420	2.090	1.115	6.117
RADIO	19.82	0.6949	0.2933	1.310	1.157	4.253	21.47	0.8114	0.1787	1.294	1.089	4.394	21.90	0.8080	0.2368	1.412	1.030	4.784	25.04	0.8790	0.1382	1.718	1.216	4.939
MAE	18.92	0.6517	0.3354	2.562	1.117	7.677	19.89	0.7696	0.2271	3.025	1.254	8.707	21.20	0.7911	0.2601	2.813	1.149	8.615	24.34	0.8736	0.1467	2.416	1.209	7.116
SD	18.99	0.6659	0.3234	3.268	1.365	9.850	19.77	0.7726	0.2285	3.799	1.500	10.761	20.83	0.7966	0.2579	4.145	1.346	12.603	24.56	0.8727	0.1511	3.176	1.275	10.012
IUVRGB	14.62	0.5387	0.4266	8.041	11.738	49.719	15.98	0.6840	0.3147	19.184	17.793	50.164	14.72	0.6881	0.3827	13.994	30.404	51.205	19.44	0.8207	0.1996	9.536	7.047	47.307
Scan10 (DTU)																								
Feature	PSNR ↑	SSIM ↑	LPIPS ↓	Acc. ↓	Comp. ↓	Dist. ↓	PSNR ↑	SSIM ↑	LPIPS ↓	Acc. ↓	Comp. ↓	Dist. ↓	PSNR ↑	SSIM ↑	LPIPS ↓	Acc. ↓	Comp. ↓	Dist. ↓	PSNR ↑	SSIM ↑	LPIPS ↓	Acc. ↓	Comp. ↓	Dist. ↓
DUS3R	19.29	0.6866	0.3106	1.860	1.140	5.944	20.53	0.7889	0.2103	2.090	1.244	6.577	21.94	0.8048	0.2495	2.304	1.094	7.266	24.76	0.8767	0.1442	2.299	1.181	6.556
MAS3R	19.38	0.6878	0.3092	1.680	1.088	5.285	20.44	0.7876	0.2117	2.103	1.242	6.230	21.68	0.8022	0.2552	2.110	1.090	6.237	24.83	0.8776	0.1431	2.209	1.235	6.413
MiDaS	19.44	0.6759	0.3179	2.412	1.200	7.370	19.78	0.7709	0.2256	3.824	1.550	10.567	21.68	0.8020	0.2488	2.770	1.160	8.400	24.12	0.8716	0.1478	2.487	1.277	7.158
DINov2	19.33	0.6791	0.3153	2.191	1.147	7.162	20.00	0.7733	0.2248	3.476	1.462	8.763	21.50	0.8039	0.2535	2.990	1.125	9.059	24.61	0.8745	0.1468	2.456	1.154	7.260
DINO	19.83	0.6904	0.3074	1.770	1.098	5.542	20.38	0.7876	0.2109	2.362	1.211	7.103	21.83	0.8019	0.2498	2.370	1.126	7.559	24.45	0.8758	0.1440	2.006	1.172	5.859
SAM	19.11	0.6650	0.3252	2.495	1.110	8.064	19.99	0.7774	0.2224	3.307	1.478	8.919	21.14	0.7897	0.2618	3.084	1.175	9.145	24.67	0.8732	0.1468	2.560	1.176	7.627
CLIP	19.33	0.6835	0.3158	1.596	1.009	5.203	20.26	0.7769	0.2193	2.338	1.180	6.781	21.76	0.8032	0.2575	2.244	1.027	7.124	24.54	0.8747	0.1420	2.090	1.115	6.117
RADIO	19.82	0.6949	0.2933	1.310	1.157	4.253	21.47	0.8114	0.1787	1.294	1.089	4.394	21.90	0.8080	0.2368	1.412	1.030	4.784	25.04	0.8790	0.1382	1.718	1.216	4.939
MAE	18.92	0.6517	0.3354	2.562	1.117	7.677	19.89	0.7696	0.2271	3.025	1.254	8.707	21.20	0.7911	0.2601	2.813	1.149	8.615	24.34	0.8736	0.1467	2.416	1.209	7.116
SD	18.99	0.6659	0.3234	3.268	1.365	9.850	19.77	0.7726	0.2285	3.799	1.500	10.761	20.83	0.7966	0.2579	4.145	1.346	12.603	24.56	0.8727	0.1511	3.176	1.275	10.012
IUVRGB	14.62	0.5387	0.4266	8.041	11.738	49.719	15.98	0.6840	0.3147	19.184	17.793	50.164	14.72	0.6881	0.3827	13.994	30.404	51.205	19.44	0.8207	0.1996	9.536	7.047	47.307
Scan11 (DTU)																								
Feature	PSNR ↑	SSIM ↑	LPIPS ↓	Acc. ↓	Comp. ↓	Dist. ↓	PSNR ↑	SSIM ↑	LPIPS ↓	Acc. ↓	Comp. ↓	Dist. ↓	PSNR ↑	SSIM ↑	LPIPS ↓	Acc. ↓	Comp. ↓	Dist. ↓	PSNR ↑	SSIM ↑	LPIPS ↓	Acc. ↓	Comp. ↓	Dist. ↓
DUS3R	19.29	0.6866	0.3106	1.860	1.140	5.944	20.53	0.7889	0.2103	2.090	1.244	6.577	21.94	0.8048	0.2495	2.304	1.094	7.266	24.76	0.8767	0.1442	2.299	1.181	6.556
MAS3R	19.38	0.6878	0.3092	1.680	1.088	5.285	20.44	0.7876	0.2117	2.103	1.242	6.230	21.68	0.8022	0.2552	2.110	1.090	6.237	24.83	0.8776	0.1431	2.209	1.235	6.413
MiDaS	19.44	0.6759	0.3179	2.412	1.200	7.370	19.78	0.7709	0.2256	3.824	1.550	10.567	21.68	0.8020	0.2488	2.770	1.160	8.400	24.12	0.8716	0.1478	2.487	1.277	7.158
DINov2	19.33	0.6791	0.3153	2.191	1.147	7.162	20.00	0.7733	0.2248	3.476	1.462	8.763	21.50	0.8039	0.2535	2.990	1.125	9.059	24.61	0.8745	0.1468	2.456	1.154	7.260
DINO	19.83	0.6904	0.3074	1.770	1.098	5.542	20.38	0.7876	0.2109	2.362	1.211	7.103	21.83	0.8019	0.2498	2.370	1.126	7.559	24.45	0.8758	0.1440	2.006	1.172	5.859
SAM	19.11	0.6650	0.3252	2.495	1.110	8.064	19.99	0.7774	0.2224	3.307	1.478	8.919	21.14	0.7897	0.2618	3.084	1.175	9.145	24.67	0.8732	0.1468	2.560	1.176	7.627
CLIP	19.33	0.6835	0.3158	1.596	1.009	5.203	20.26	0.7769	0.2193	2.338	1.180	6.781	21.76	0.8032	0.2575	2.244	1.027	7.124	24.54	0.8747	0.1420	2.090	1.115	6.117
RADIO	19.82	0.6949	0.2933	1.310	1.157	4.253	21.47	0.8114	0.1787	1.294	1.089	4.394	21.90	0.8080	0.2368	1.412	1.030	4.784	25.04	0.8790	0.1382	1.718	1.216	4.939
MAE	18.92	0.6517	0.3354	2.562	1.117	7.677	19.89	0.7696	0.2271	3.025	1.254	8.707	21.20	0.7911	0.2601	2.813	1.149	8.615	24.34	0.8736	0.1467	2.416	1.209	7.116
SD	18.99	0.6659	0.3234	3.268	1.365	9.850	19.77	0.7726	0.2285	3.799	1.500	10.761	20.83	0.7966	0.2579	4.145	1.346	12.603	24.56	0.8727	0.1511	3.176	1.275	10.012
IUVRGB	14.62	0.5387	0.4266	8.041	11.738	49.719	15.98	0.6840	0.3147	19.184	17.793	50.164												

References

- [1] Henrik Aanæs, Rasmus Ramsbøl Jensen, George Vogiatzis, Engin Tola, and Anders Bjarholm Dahl. Large-scale data for multiple-view stereopsis. *International Journal of Computer Vision*, 120:153–168, 2016. 4, 5, 6
- [2] Görkay Aydemir, Weidi Xie, and Fatma Güney. Can visual foundation models achieve long-term point tracking? *arXiv preprint arXiv:2408.13575*, 2024. 2, 3
- [3] Gwangbin Bae and Andrew J. Davison. Rethinking inductive biases for surface normal estimation. In *IEEE/CVF Conference on Computer Vision and Pattern Recognition (CVPR)*, 2024. 1, 2
- [4] Jonathan T Barron, Ben Mildenhall, Dor Verbin, Pratul P Srinivasan, and Peter Hedman. Mip-nerf 360: Unbounded anti-aliased neural radiance fields. In *Proceedings of the IEEE/CVF conference on computer vision and pattern recognition*, pages 5470–5479, 2022. 2, 4
- [5] Wenjing Bian, Zirui Wang, Kejie Li, Jia-Wang Bian, and Victor Adrian Prisacariu. Nope-nerf: Optimising neural radiance field with no pose prior. In *Proceedings of the IEEE/CVF Conference on Computer Vision and Pattern Recognition*, pages 4160–4169, 2023. 3
- [6] Rishi Bommasani, Drew A Hudson, Ehsan Adeli, Russ Altman, Simran Arora, Sydney von Arx, Michael S Bernstein, Jeannette Bohg, Antoine Bosselut, Emma Brunskill, et al. On the opportunities and risks of foundation models. *arXiv preprint arXiv:2108.07258*, 2021. 1, 2
- [7] Tyler Bonnen, Stephanie Fu, Yutong Bai, Thomas O’Connell, Yoni Friedman, Nancy Kanwisher, Joshua B. Tenenbaum, and Alexei A. Efros. Evaluating multiview object consistency in humans and image models, 2024. 3
- [8] Eric Brachmann, Jamie Wynn, Shuai Chen, Tommaso Cavallari, Áron Monzpárt, Daniyar Turmukhambetov, and Victor Adrian Prisacariu. Scene coordinate reconstruction: Posing of image collections via incremental learning of a relocalizer. In *ECCV*, 2024. 2, 8, 10
- [9] Mathilde Caron, Hugo Touvron, Ishan Misra, Hervé Jégou, Julien Mairal, Piotr Bojanowski, and Armand Joulin. Emerging properties in self-supervised vision transformers. In *Proceedings of the IEEE/CVF international conference on computer vision*, pages 9650–9660, 2021. 1, 2, 3, 4, 5, 6, 7, 11
- [10] David Charatan, Sizhe Lester Li, Andrea Tagliasacchi, and Vincent Sitzmann. pixelsplat: 3d gaussian splats from image pairs for scalable generalizable 3d reconstruction. In *Proceedings of the IEEE/CVF Conference on Computer Vision and Pattern Recognition*, pages 19457–19467, 2024. 1, 3
- [11] Anpei Chen, Zexiang Xu, Andreas Geiger, Jingyi Yu, and Hao Su. Tensorf: Tensorial radiance fields. In *European Conference on Computer Vision (ECCV)*, 2022. 3
- [12] Anpei Chen, Haofei Xu, Stefano Esposito, Siyu Tang, and Andreas Geiger. Lara: Efficient large-baseline radiance fields. In *European Conference on Computer Vision (ECCV)*, 2024. 3
- [13] Boyuan Chen, Zhuo Xu, Sean Kirmani, Brain Ichter, Dorsa Sadigh, Leonidas Guibas, and Fei Xia. Spatialvlm: Endowing vision-language models with spatial reasoning capabilities. In *Proceedings of the IEEE/CVF Conference on Computer Vision and Pattern Recognition*, pages 14455–14465, 2024. 1, 2
- [14] Ting Chen, Simon Kornblith, Mohammad Norouzi, and Geoffrey Hinton. A simple framework for contrastive learning of visual representations. In *Proceedings of the 37th International Conference on Machine Learning*, pages 1597–1607. PMLR, 2020. 7
- [15] Xingyu Chen, Qi Zhang, Xiaoyu Li, Yue Chen, Ying Feng, Xuan Wang, and Jue Wang. Hallucinated neural radiance fields in the wild. In *Proceedings of the IEEE/CVF Conference on Computer Vision and Pattern Recognition*, pages 12943–12952, 2022. 10
- [16] Yue Chen, Xingyu Chen, Xuan Wang, Qi Zhang, Yu Guo, Ying Shan, and Fei Wang. Local-to-global registration for bundle-adjusting neural radiance fields. In *Proceedings of the IEEE/CVF Conference on Computer Vision and Pattern Recognition*, pages 8264–8273, 2023. 3
- [17] Yuedong Chen, Haofei Xu, Chuanxia Zheng, Bohan Zhuang, Marc Pollefeys, Andreas Geiger, Tat-Jen Cham, and Jianfei Cai. Mvsplat: Efficient 3d gaussian splatting from sparse multi-view images. *ECCV*, 2024. 3
- [18] Timothée Darcet, Maxime Oquab, Julien Mairal, and Piotr Bojanowski. Vision transformers need registers. In *The Twelfth International Conference on Learning Representations*, 2024. 11
- [19] Matt Deitke, Dustin Schwenk, Jordi Salvador, Luca Weihs, Oscar Michel, Eli VanderBilt, Ludwig Schmidt, Kiana Ehsani, Aniruddha Kembhavi, and Ali Farhadi. Objaverse: A universe of annotated 3d objects. In *Proceedings of the IEEE/CVF Conference on Computer Vision and Pattern Recognition*, pages 13142–13153, 2023. 11, 13
- [20] Kangle Deng, Andrew Liu, Jun-Yan Zhu, and Deva Ramanan. Depth-supervised nerf: Fewer views and faster training for free. In *Proceedings of the IEEE/CVF Conference on Computer Vision and Pattern Recognition*, pages 12882–12891, 2022. 3
- [21] Mohamed El Banani, Amit Raj, Kevis-Kokitsi Maninis, Abhishek Kar, Yuanzhen Li, Michael Rubinstein, Deqing Sun, Leonidas Guibas, Justin Johnson, and Varun Jampani. Probing the 3d awareness of visual foundation models. In *Proceedings of the IEEE/CVF Conference on Computer Vision and Pattern Recognition*, pages 21795–21806, 2024. 2, 3, 7, 11
- [22] Zhiwen Fan, Wenyan Cong, Kairun Wen, Kevin Wang, Jian Zhang, Xinghao Ding, Danfei Xu, Boris Ivanovic, Marco Pavone, Georgios Pavlakos, et al. Instantsplat: Unbounded sparse-view pose-free gaussian splatting in 40 seconds. *arXiv preprint arXiv:2403.20309*, 2024. 2, 3, 4, 9
- [23] Zhiwen Fan, Jian Zhang, Wenyan Cong, Peihao Wang, Renjie Li, Kairun Wen, Shijie Zhou, Achuta Kadambi, Zhangyang Wang, Danfei Xu, et al. Large spatial model: End-to-end unposed images to semantic 3d. *NeurIPS*, 2024. 2, 3, 10
- [24] Yao Feng, Jing Lin, Sai Kumar Dwivedi, Yu Sun, Priyanka Patel, and Michael J Black. Chatpose: Chatting about 3d human pose. In *Proceedings of the IEEE/CVF Conference*

- on *Computer Vision and Pattern Recognition*, pages 2093–2103, 2024. [2](#)
- [25] Stephanie Fu, Mark Hamilton, Laura E. Brandt, Axel Feldmann, Zhoutong Zhang, and William T. Freeman. Featup: A model-agnostic framework for features at any resolution. In *The Twelfth International Conference on Learning Representations*, 2024. [10](#), [11](#), [13](#)
- [26] Xingyu Fu, Yushi Hu, Bangzheng Li, Yu Feng, Haoyu Wang, Xudong Lin, Dan Roth, Noah A Smith, Wei-Chiu Ma, and Ranjay Krishna. Blink: Multimodal large language models can see but not perceive. 2024. [3](#)
- [27] Xiao Fu, Wei Yin, Mu Hu, Kaixuan Wang, Yuexin Ma, Ping Tan, Shaojie Shen, Dahua Lin, and Xiaoxiao Long. Geowizard: Unleashing the diffusion priors for 3d geometry estimation from a single image. In *ECCV*, 2024. [2](#)
- [28] Yang Fu, Sifei Liu, Amey Kulkarni, Jan Kautz, Alexei A. Efros, and Xiaolong Wang. Colmap-free 3d gaussian splatting. In *Proceedings of the IEEE/CVF Conference on Computer Vision and Pattern Recognition (CVPR)*, pages 20796–20805, 2024. [3](#)
- [29] Robert Geirhos, Patricia Rubisch, Claudio Michaelis, Matthias Bethge, Felix A Wichmann, and Wieland Brendel. Imagenet-trained CNNs are biased towards texture; increasing shape bias improves accuracy and robustness. In *International Conference on Learning Representations*, 2019. [7](#)
- [30] Robert Geirhos, Jörn-Henrik Jacobsen, Claudio Michaelis, Richard Zemel, Wieland Brendel, Matthias Bethge, and Felix A Wichmann. Shortcut learning in deep neural networks. *Nature Machine Intelligence*, 2(11):665–673, 2020. [7](#)
- [31] Jean-Bastien Grill, Florian Strub, Florent Altché, Corentin Tallec, Pierre Richemond, Elena Buchatskaya, Carl Doersch, Bernardo Avila Pires, Zhaohan Guo, Mohammad Gheshlaghi Azar, et al. Bootstrap your own latent—a new approach to self-supervised learning. *Advances in neural information processing systems*, 33:21271–21284, 2020. [7](#)
- [32] Nathan Halko, Per-Gunnar Martinsson, and Joel A Tropp. Finding structure with randomness: Probabilistic algorithms for constructing approximate matrix decompositions. *SIAM review*, 53(2):217–288, 2011. [3](#)
- [33] Kaiming He, Xinlei Chen, Saining Xie, Yanghao Li, Piotr Dollár, and Ross Girshick. Masked autoencoders are scalable vision learners. In *Proceedings of the IEEE/CVF conference on computer vision and pattern recognition*, pages 16000–16009, 2022. [2](#), [4](#), [5](#), [6](#), [8](#), [10](#), [11](#), [12](#)
- [34] Yicong Hong, Kai Zhang, Jiuxiang Gu, Sai Bi, Yang Zhou, Difan Liu, Feng Liu, Kalyan Sunkavalli, Trung Bui, and Hao Tan. Lrm: Large reconstruction model for single image to 3d. *ICLR*, 2024. [1](#), [2](#), [3](#)
- [35] Wenbo Hu, Xiangjun Gao, Xiaoyu Li, Sijie Zhao, Xiaodong Cun, Yong Zhang, Long Quan, and Ying Shan. Depthrafter: Generating consistent long depth sequences for open-world videos. *arXiv preprint arXiv:2409.02095*, 2024. [2](#)
- [36] Ajay Jain, Matthew Tancik, and Pieter Abbeel. Putting nerf on a diet: Semantically consistent few-shot view synthesis. In *Proceedings of the IEEE/CVF International Conference on Computer Vision (ICCV)*, pages 5885–5894, 2021. [3](#)
- [37] Yoonwoo Jeong, Seokjun Ahn, Christopher Choy, Anima Anandkumar, Minsu Cho, and Jaesik Park. Self-calibrating neural radiance fields. In *Proceedings of the IEEE/CVF International Conference on Computer Vision*, pages 5846–5854, 2021. [3](#)
- [38] Haian Jin, Hanwen Jiang, Hao Tan, Kai Zhang, Sai Bi, Tianyuan Zhang, Fujun Luan, Noah Snavely, and Zexiang Xu. Lvsm: A large view synthesis model with minimal 3d inductive bias, 2024. [3](#)
- [39] Bingxin Ke, Anton Obukhov, Shengyu Huang, Nando Metzger, Rodrigo Caye Daudt, and Konrad Schindler. Repurposing diffusion-based image generators for monocular depth estimation. In *Proceedings of the IEEE/CVF Conference on Computer Vision and Pattern Recognition*, pages 9492–9502, 2024. [1](#), [2](#)
- [40] Bernhard Kerbl, Georgios Kopanas, Thomas Leimkühler, and George Drettakis. 3d gaussian splatting for real-time radiance field rendering. *ACM Transactions on Graphics*, 42(4), 2023. [2](#), [3](#), [5](#), [11](#)
- [41] Justin* Kerr, Chung Min* Kim, Ken Goldberg, Angjoo Kanazawa, and Matthew Tancik. Lrf: Language embedded radiance fields. In *International Conference on Computer Vision (ICCV)*, 2023. [3](#)
- [42] Rawal Khrodgar, Timur Bagautdinov, Julieta Martinez, Su Zhaoen, Austin James, Peter Selednik, Stuart Anderson, and Shunsuke Saito. Sapiens: Foundation for human vision models. In *ECCV*, 2024. [2](#)
- [43] Chung Min Kim, Mingxuan Wu, Justin Kerr, Ken Goldberg, Matthew Tancik, and Angjoo Kanazawa. Garfield: Group anything with radiance fields. In *Proceedings of the IEEE/CVF Conference on Computer Vision and Pattern Recognition*, pages 21530–21539, 2024. [3](#)
- [44] Alexander Kirillov, Eric Mintun, Nikhila Ravi, Hanzi Mao, Chloe Rolland, Laura Gustafson, Tete Xiao, Spencer Whitehead, Alexander C Berg, Wan-Yen Lo, et al. Segment anything. In *Proceedings of the IEEE/CVF International Conference on Computer Vision*, pages 4015–4026, 2023. [1](#), [2](#), [3](#), [4](#), [5](#), [6](#), [11](#)
- [45] James Kirkpatrick, Razvan Pascanu, Neil Rabinowitz, Joel Veness, Guillaume Desjardins, Andrei A Rusu, Kieran Milan, John Quan, Tiago Ramalho, Agnieszka Grabska-Barwinska, et al. Overcoming catastrophic forgetting in neural networks. *Proceedings of the national academy of sciences*, 114(13):3521–3526, 2017. [11](#), [13](#)
- [46] Arno Knapitsch, Jaesik Park, Qian-Yi Zhou, and Vladlen Koltun. Tanks and temples: Benchmarking large-scale scene reconstruction. *ACM Transactions on Graphics (ToG)*, 36(4):1–13, 2017. [2](#), [4](#)
- [47] Sosuke Kobayashi, Eiichi Matsumoto, and Vincent Sitzmann. Decomposing nerf for editing via feature field distillation. In *Advances in Neural Information Processing Systems*, 2022. [3](#)
- [48] Jonas Kulhanek, Songyou Peng, Zuzana Kukelova, Marc Pollefeys, and Torsten Sattler. Wildgaussians: 3d gaussian splatting in the wild. *arXiv preprint arXiv:2407.08447*, 2024. [10](#)

- [49] Vincent Leroy, Yohann Cabon, and Jerome Revaud. Grounding image matching in 3d with mast3r, 2024. [2](#), [3](#), [4](#), [5](#), [6](#), [10](#), [11](#)
- [50] Boyi Li, Kilian Q Weinberger, Serge Belongie, Vladlen Koltun, and Rene Ranftl. Language-driven semantic segmentation. In *International Conference on Learning Representations*, 2022. [3](#)
- [51] Chen-Hsuan Lin, Wei-Chiu Ma, Antonio Torralba, and Simon Lucey. Barf: Bundle-adjusting neural radiance fields. In *Proceedings of the IEEE/CVF international conference on computer vision*, pages 5741–5751, 2021. [3](#), [4](#)
- [52] Lu Ling, Yichen Sheng, Zhi Tu, Wentian Zhao, Cheng Xin, Kun Wan, Lantao Yu, Qianyu Guo, Zixun Yu, Yawen Lu, et al. D13dv-10k: A large-scale scene dataset for deep learning-based 3d vision. In *Proceedings of the IEEE/CVF Conference on Computer Vision and Pattern Recognition*, pages 22160–22169, 2024. [2](#), [4](#)
- [53] Drew Linsley, Peisen Zhou, Alekh Karkada Ashok, Akash Nagaraj, Gaurav Gaonkar, Francis E Lewis, Zygmunt Pizlo, and Thomas Serre. The 3d-pc: a benchmark for visual perspective taking in humans and machines. *arXiv preprint arXiv:2406.04138*, 2024. [3](#)
- [54] Ruoshi Liu, Rundi Wu, Basile Van Hoorick, Pavel Tokmakov, Sergey Zakharov, and Carl Vondrick. Zero-1-to-3: Zero-shot one image to 3d object. In *Proceedings of the IEEE/CVF international conference on computer vision*, pages 9298–9309, 2023. [3](#)
- [55] Jonathon Luiten, Georgios Kopanas, Bastian Leibe, and Deva Ramanan. Dynamic 3d gaussians: Tracking by persistent dynamic view synthesis. In *3DV*, 2024. [10](#)
- [56] Arjun Majumdar, Karmesh Yadav, Sergio Arnaud, Jason Ma, Claire Chen, Sneha Silwal, Aryan Jain, Vincent-Pierre Berges, Tingfan Wu, Jay Vakil, et al. Where are we in the search for an artificial visual cortex for embodied intelligence? *Advances in Neural Information Processing Systems*, 36:655–677, 2023. [3](#)
- [57] Ricardo Martin-Brualla, Noha Radwan, Mehdi SM Sajjadi, Jonathan T Barron, Alexey Dosovitskiy, and Daniel Duckworth. Nerf in the wild: Neural radiance fields for unconstrained photo collections. In *Proceedings of the IEEE/CVF conference on computer vision and pattern recognition*, pages 7210–7219, 2021. [10](#)
- [58] Quan Meng, Anpei Chen, Haimin Luo, Minye Wu, Hao Su, Lan Xu, Xuming He, and Jingyi Yu. GNeRF: GAN-based Neural Radiance Field without Posed Camera. In *Proceedings of the IEEE/CVF International Conference on Computer Vision (ICCV)*, 2021. [3](#)
- [59] Andreas Meuleman, Yu-Lun Liu, Chen Gao, Jia-Bin Huang, Changil Kim, Min H Kim, and Johannes Kopf. Progressively optimized local radiance fields for robust view synthesis. In *Proceedings of the IEEE/CVF Conference on Computer Vision and Pattern Recognition*, pages 16539–16548, 2023. [3](#)
- [60] Ben Mildenhall, Pratul P. Srinivasan, Rodrigo Ortiz-Cayon, Nima Khademi Kalantari, Ravi Ramamoorthi, Ren Ng, and Abhishek Kar. Local light field fusion: Practical view synthesis with prescriptive sampling guidelines. *ACM Transactions on Graphics (TOG)*, 2019. [2](#), [4](#)
- [61] Ben Mildenhall, Pratul P. Srinivasan, Matthew Tancik, Jonathan T. Barron, Ravi Ramamoorthi, and Ren Ng. Nerf: Representing scenes as neural radiance fields for view synthesis. In *ECCV*, 2020. [3](#)
- [62] Thomas Müller, Alex Evans, Christoph Schied, and Alexander Keller. Instant neural graphics primitives with a multiresolution hash encoding. *ACM Trans. Graph.*, 41(4):102:1–102:15, 2022. [3](#)
- [63] Michael Niemeyer, Jonathan T Barron, Ben Mildenhall, Mehdi SM Sajjadi, Andreas Geiger, and Noha Radwan. Regnerf: Regularizing neural radiance fields for view synthesis from sparse inputs. In *Proceedings of the IEEE/CVF Conference on Computer Vision and Pattern Recognition*, pages 5480–5490, 2022. [3](#)
- [64] Maxime Oquab, Timothée Darcet, Théo Moutakanni, Huy Vo, Marc Szafraniec, Vasil Khalidov, Pierre Fernandez, Daniel Haziza, Francisco Massa, Alaaeldin El-Nouby, et al. Dinov2: Learning robust visual features without supervision. *arXiv preprint arXiv:2304.07193*, 2023. [4](#), [5](#), [6](#), [11](#)
- [65] Evin Pinar Örnek, Yann Labbé, Bugra Tekin, Lingni Ma, Cem Keskin, Christian Forster, and Tomáš Hodaň. Foundpose: Unseen object pose estimation with foundation features. *ECCV*, 2024. [2](#), [10](#)
- [66] Adam Paszke, Sam Gross, Francisco Massa, Adam Lerer, James Bradbury, Gregory Chanan, Trevor Killeen, Zeming Lin, Natalia Gimelshein, Luca Antiga, et al. Pytorch: An imperative style, high-performance deep learning library. *Advances in neural information processing systems*, 32, 2019. [5](#)
- [67] Songyou Peng, Kyle Genova, Chiyu “Max” Jiang, Andrea Tagliasacchi, Marc Pollefeys, and Thomas Funkhouser. Openscene: 3d scene understanding with open vocabularies. In *CVPR*, 2023. [3](#)
- [68] Minghan Qin, Wanhua Li, Jiawei Zhou, Haoqian Wang, and Hanspeter Pfister. Langsplat: 3d language gaussian splatting. In *Proceedings of the IEEE/CVF Conference on Computer Vision and Pattern Recognition*, pages 20051–20060, 2024. [3](#)
- [69] Alec Radford, Jong Wook Kim, Chris Hallacy, Aditya Ramesh, Gabriel Goh, Sandhini Agarwal, Girish Sastry, Amanda Askell, Pamela Mishkin, Jack Clark, et al. Learning transferable visual models from natural language supervision. In *International conference on machine learning*, pages 8748–8763. PMLR, 2021. [1](#), [3](#), [4](#), [5](#), [6](#), [11](#)
- [70] René Ranftl, Katrin Lasinger, David Hafner, Konrad Schindler, and Vladlen Koltun. Towards robust monocular depth estimation: Mixing datasets for zero-shot cross-dataset transfer. *IEEE transactions on pattern analysis and machine intelligence*, 44(3):1623–1637, 2020. [1](#), [2](#), [4](#), [5](#), [6](#), [11](#)
- [71] René Ranftl, Alexey Bochkovskiy, and Vladlen Koltun. Vision transformers for dense prediction. In *Proceedings of the IEEE/CVF international conference on computer vision*, pages 12179–12188, 2021. [11](#)
- [72] Mike Ranzinger, Greg Heinrich, Jan Kautz, and Pavlo Molchanov. Am-radio: Agglomerative vision foundation model reduce all domains into one. In *Proceedings of the*

- IEEE/CVF Conference on Computer Vision and Pattern Recognition (CVPR)*, pages 12490–12500, 2024. [1](#), [4](#), [5](#), [6](#), [10](#), [11](#)
- [73] Nikhila Ravi, Valentin Gabeur, Yuan-Ting Hu, Ronghang Hu, Chaitanya Ryalí, Tengyu Ma, Haitham Khedr, Roman Rädle, Chloe Rolland, Laura Gustafson, et al. Sam 2: Segment anything in images and videos. *arXiv preprint arXiv:2408.00714*, 2024. [3](#)
- [74] Arijit Ray, Dina Bashkirova, Reuben Tan, Kuo-Hao Zeng, Bryan A Plummer, Ranjay Krishna, and Kate Saenko. R2d3: Imparting spatial reasoning by reconstructing 3d scenes from 2d images. [2](#), [3](#)
- [75] Robin Rombach, Andreas Blattmann, Dominik Lorenz, Patrick Esser, and Björn Ommer. High-resolution image synthesis with latent diffusion models. In *Proceedings of the IEEE/CVF conference on computer vision and pattern recognition*, pages 10684–10695, 2022. [1](#), [2](#), [3](#), [4](#), [5](#), [6](#), [11](#)
- [76] Kyle Sargent, Zizhang Li, Tanmay Shah, Charles Herrmann, Hong-Xing Yu, Yunzhi Zhang, Eric Ryan Chan, Dmitry Lagun, Li Fei-Fei, Deqing Sun, et al. Zeronvs: Zero-shot 360-degree view synthesis from a single image. In *Proceedings of the IEEE/CVF Conference on Computer Vision and Pattern Recognition*, pages 9420–9429, 2024. [3](#)
- [77] Johannes Lutz Schönberger and Jan-Michael Frahm. Structure-from-motion revisited. In *Conference on Computer Vision and Pattern Recognition (CVPR)*, 2016. [3](#)
- [78] Jinghuan Shang, Karl Schmeckpeper, Brandon B. May, Maria Vittoria Minniti, Tarik Kelestemur, David Watkins, and Laura Herlant. Theia: Distilling diverse vision foundation models for robot learning. In *8th Annual Conference on Robot Learning*, 2024. [3](#), [10](#)
- [79] Jamie Shotton, Ben Glocker, Christopher Zach, Shahram Izadi, Antonio Criminisi, and Andrew Fitzgibbon. Scene coordinate regression forests for camera relocalization in rgb-d images. In *Proceedings of the IEEE conference on computer vision and pattern recognition*, pages 2930–2937, 2013. [8](#)
- [80] Yawar Siddiqui, Lorenzo Porzi, Samuel Rota Buló, Norman Müller, Matthias Nießner, Angela Dai, and Peter Kotschieder. Panoptic lifting for 3d scene understanding with neural fields. In *Proceedings of the IEEE/CVF Conference on Computer Vision and Pattern Recognition*, pages 9043–9052, 2023. [3](#)
- [81] Brandon Smart, Chuanxia Zheng, Iro Laina, and Victor Adrian Prisacariu. Splatt3r: Zero-shot gaussian splatting from uncalibrated image pairs. *arXiv preprint arXiv:2408.13912*, 2024. [2](#), [3](#), [4](#), [7](#)
- [82] Cameron Smith, David Charatan, Ayush Tewari, and Vincent Sitzmann. Flowmap: High-quality camera poses, intrinsics, and depth via gradient descent. *arXiv preprint arXiv:2404.15259*, 2024. [2](#)
- [83] Noah Snavely, Steven M Seitz, and Richard Szeliski. Photo tourism: exploring photo collections in 3d. In *ACM siggraph 2006 papers*, pages 835–846. 2006. [10](#)
- [84] Saksham Suri, Matthew Walmer, Kamal Gupta, and Abhinav Shrivastava. Lift: A surprisingly simple lightweight feature transform for dense vit descriptors. In *European Conference on Computer Vision*, pages 110–128. Springer, 2025. [10](#)
- [85] Matthew Tancik, Ethan Weber, Evonne Ng, Ruilong Li, Brent Yi, Justin Kerr, Terrance Wang, Alexander Kristoffersen, Jake Austin, Kamyar Salahi, Abhik Ahuja, David McAllister, and Angjoo Kanazawa. Nerfstudio: A modular framework for neural radiance field development. In *ACM SIGGRAPH 2023 Conference Proceedings*, 2023. [3](#)
- [86] Prune Truong, Marie-Julie Rakotosaona, Fabian Manhardt, and Federico Tombari. Sparf: Neural radiance fields from sparse and noisy poses. In *Proceedings of the IEEE/CVF Conference on Computer Vision and Pattern Recognition*, pages 4190–4200, 2023. [3](#)
- [87] Vadim Tschernezki, Iro Laina, Diane Larlus, and Andrea Vedaldi. Neural Feature Fusion Fields: 3D distillation of self-supervised 2D image representations. In *Proceedings of the International Conference on 3D Vision (3DV)*, 2022. [3](#)
- [88] Narek Tumanyan, Assaf Singer, Shai Bagon, and Tali Dekel. Dino-tracker: Taming dino for self-supervised point tracking in a single video. In *European Conference on Computer Vision (ECCV)*, 2024. [2](#)
- [89] Joseph Tung, Gene Chou, Ruojin Cai, Guandao Yang, Kai Zhang, Gordon Wetzstein, Bharath Hariharan, and Noah Snavely. Megascenes: Scene-level view synthesis at scale. In *ECCV*, 2024. [3](#), [10](#)
- [90] Can Wang, Menglei Chai, Mingming He, Dongdong Chen, and Jing Liao. Clip-nerf: Text-and-image driven manipulation of neural radiance fields. *arXiv preprint arXiv:2112.05139*, 2021. [3](#)
- [91] Hengyi Wang and Lourdes Agapito. 3d reconstruction with spatial memory. *arXiv preprint arXiv:2408.16061*, 2024. [3](#), [4](#), [5](#), [10](#)
- [92] Qixun Wang, Xu Bai, Haofan Wang, Zekui Qin, and Anthony Chen. Instantid: Zero-shot identity-preserving generation in seconds. *arXiv preprint arXiv:2401.07519*, 2024. [7](#)
- [93] Qianqian Wang, Vickie Ye, Hang Gao, Jake Austin, Zhengqi Li, and Angjoo Kanazawa. Shape of motion: 4d reconstruction from a single video. *arXiv e-prints*, pages arXiv–2407, 2024. [10](#)
- [94] Shuzhe Wang, Vincent Leroy, Yohann Cabon, Boris Chidlovskii, and Jerome Revaud. Dust3r: Geometric 3d vision made easy. In *Proceedings of the IEEE/CVF Conference on Computer Vision and Pattern Recognition (CVPR)*, pages 20697–20709, 2024. [1](#), [2](#), [3](#), [4](#), [5](#), [6](#), [8](#), [10](#), [11](#)
- [95] Zirui Wang, Shangzhe Wu, Weidi Xie, Min Chen, and Victor Adrian Prisacariu. NeRF—: Neural radiance fields without known camera parameters. *arXiv preprint arXiv:2102.07064*, 2021. [3](#)
- [96] Frederik Warburg*, Ethan Weber*, Matthew Tancik, Aleksander Hołyński, and Angjoo Kanazawa. Nerfbusters: Removing ghostly artifacts from casually captured nerfs. In *International Conference on Computer Vision (ICCV)*, 2023. [3](#)
- [97] Philippe Weinzaepfel, Vincent Leroy, Thomas Lucas, Romain Brégier, Yohann Cabon, Vaibhav Arora, Leonid Antsfeld, Boris Chidlovskii, Gabriela Csurka, and Jérôme Revaud. Croco: Self-supervised pre-training for 3d vision tasks by cross-view completion. *Advances in Neural Information Processing Systems*, 35:3502–3516, 2022. [2](#), [12](#)

- [98] Rundi Wu, Ben Mildenhall, Philipp Henzler, Keunhong Park, Ruiqi Gao, Daniel Watson, Pratul P Srinivasan, Dor Verbin, Jonathan T Barron, Ben Poole, et al. Reconfusion: 3d reconstruction with diffusion priors. In *Proceedings of the IEEE/CVF Conference on Computer Vision and Pattern Recognition*, pages 21551–21561, 2024. 3
- [99] Yiheng Xie, Towaki Takikawa, Shunsuke Saito, Or Litany, Shiqin Yan, Numair Khan, Federico Tombari, James Tompkin, Vincent Sitzmann, and Srinath Sridhar. Neural fields in visual computing and beyond. In *Computer Graphics Forum*, pages 641–676. Wiley Online Library, 2022. 3
- [100] Congrong Xu, Justin Kerr, and Angjoo Kanazawa. Splatfacto-w: A nerfstudio implementation of gaussian splatting for unconstrained photo collections. *arXiv preprint arXiv:2407.12306*, 2024. 10
- [101] Dejia Xu, Yifan Jiang, Peihao Wang, Zhiwen Fan, Humphrey Shi, and Zhangyang Wang. Sinnerf: Training neural radiance fields on complex scenes from a single image. 2022. 3
- [102] Jiawei Yang, Marco Pavone, and Yue Wang. Freenerf: Improving few-shot neural rendering with free frequency regularization. In *Proceedings of the IEEE/CVF conference on computer vision and pattern recognition*, pages 8254–8263, 2023. 3
- [103] Jiawei Yang, Boris Ivanovic, Or Litany, Xinshuo Weng, Seung Wook Kim, Boyi Li, Tong Che, Danfei Xu, Sanja Fidler, Marco Pavone, et al. Emernerf: Emergent spatial-temporal scene decomposition via self-supervision. In *International Conference on Learning Representations*, 2024. 11
- [104] Jiawei Yang, Katie Z Luo, Jiefeng Li, Congyue Deng, Leonidas J. Guibas, Dilip Krishnan, Kilian Q Weinberger, Yonglong Tian, and Yue Wang. Dvt: Denoising vision transformers. 2024. 11
- [105] Botao Ye, Sifei Liu, Haoifei Xu, Xueting Li, Marc Pollefeys, Ming-Hsuan Yang, and Songyou Peng. No pose, no problem: Surprisingly simple 3d gaussian splats from sparse unposed images, 2024. 2, 3, 7, 10
- [106] Chongjie Ye, Lingteng Qiu, Xiaodong Gu, Qi Zuo, Yushuang Wu, Zilong Dong, Liefeng Bo, Yuliang Xiu, and Xiaoguang Han. Stablenormal: Reducing diffusion variance for stable and sharp normal. *ACM Transactions on Graphics (TOG)*, 2024. 1, 2
- [107] Jianglong Ye, Naiyan Wang, and Xiaolong Wang. Featurenerf: Learning generalizable nerfs by distilling foundation models. In *Proceedings of the IEEE/CVF International Conference on Computer Vision*, pages 8962–8973, 2023. 3
- [108] Mingqiao Ye, Martin Danelljan, Fisher Yu, and Lei Ke. Gaussian grouping: Segment and edit anything in 3d scenes. In *European Conference on Computer Vision*, pages 162–179. Springer, 2025. 3
- [109] Vickie Ye, Ruilong Li, Justin Kerr, Matias Turkulainen, Brent Yi, Zhuoyang Pan, Otto Seiskari, Jianbo Ye, Jeffrey Hu, Matthew Tancik, and Angjoo Kanazawa. gsplat: An open-source library for Gaussian splatting. *arXiv preprint arXiv:2409.06765*, 2024. 5
- [110] Alex Yu, Vickie Ye, Matthew Tancik, and Angjoo Kanazawa. pixelNeRF: Neural radiance fields from one or few images. In *CVPR*, 2021. 3
- [111] Xianggang Yu, Mutian Xu, Yidan Zhang, Haolin Liu, Chongjie Ye, Yushuang Wu, Zizheng Yan, Chenming Zhu, Zhangyang Xiong, Tianyou Liang, et al. Mvimngnet: A large-scale dataset of multi-view images. In *Proceedings of the IEEE/CVF conference on computer vision and pattern recognition*, pages 9150–9161, 2023. 2, 4
- [112] Yuanwen Yue, Anurag Das, Francis Engelmann, Siyu Tang, and Jan Eric Lenssen. Improving 2D Feature Representations by 3D-Aware Fine-Tuning. In *European Conference on Computer Vision (ECCV)*, 2024. 11
- [113] Dongbin Zhang, Chuming Wang, Weitao Wang, Peihao Li, Minghan Qin, and Haoqian Wang. Gaussian in the wild: 3d gaussian splatting for unconstrained image collections. In *European Conference on Computer Vision*, pages 341–359. Springer, 2025. 10
- [114] Junyi Zhang, Charles Herrmann, Junhwa Hur, Varun Jampani, Trevor Darrell, Forrester Cole, Deqing Sun, and Ming-Hsuan Yang. Monst3r: A simple approach for estimating geometry in the presence of motion. *arXiv preprint arxiv:2410.03825*, 2024. 3, 4, 10
- [115] Xiaoshuai Zhang, Zhicheng Wang, Howard Zhou, Soham Ghosh, Danushen Gnanapragasam, Varun Jampani, Hao Su, and Leonidas Guibas. Condense: Consistent 2d/3d pre-training for dense and sparse features from multi-view images. In *European Conference on Computer Vision*. Springer, 2024. 11
- [116] Shuaifeng Zhi, Tristan Laidlow, Stefan Leutenegger, and Andrew J Davison. In-place scene labelling and understanding with implicit scene representation. In *Proceedings of the IEEE/CVF International Conference on Computer Vision*, pages 15838–15847, 2021. 3
- [117] Shijie Zhou, Haoran Chang, Sicheng Jiang, Zhiwen Fan, Zehao Zhu, Dejia Xu, Pradyumna Chari, Suya You, Zhangyang Wang, and Achuta Kadambi. Feature 3dgs: Supercharging 3d gaussian splatting to enable distilled feature fields. In *Proceedings of the IEEE/CVF Conference on Computer Vision and Pattern Recognition*, pages 21676–21685, 2024. 3
- [118] Haoyi Zhu, Honghui Yang, Yating Wang, Jiange Yang, Limin Wang, and Tong He. Spa: 3d spatial-awareness enables effective embodied representation. *arXiv preprint arXiv:2410.08208*, 2024. 3
- [119] Zehao Zhu, Zhiwen Fan, Yifan Jiang, and Zhangyang Wang. Fsgs: Real-time few-shot view synthesis using gaussian splatting, 2023. 3
- [120] Chen Ziwen, Hao Tan, Kai Zhang, Sai Bi, Fujun Luan, Yicong Hong, Li Fuxin, and Zexiang Xu. Long-irm: Long-sequence large reconstruction model for wide-coverage gaussian splats. *arXiv preprint 2410.12781*, 2024. 3
- [121] Yiming Zuo, Karhan Kayan, Maggie Wang, Kevin Jeon, Jia Deng, and Thomas L Griffiths. Towards foundation models for 3d vision: How close are we? *arXiv preprint arXiv:2410.10799*, 2024. 3